Combustion and Flame 158 (2011) 774–789

Contents lists available at ScienceDirect

Combustion and Flame

journal homepage: www.elsevier.com/locate/combustflame

The role of NNH in NO formation and control

Stephen J. Klippenstein [a], Lawrence B. Harding [a], Peter Glarborg [b,*], James A. Miller [c]

[a] Chemical Sciences and Engineering Division, Argonne National Laboratory, Argonne, IL 60439, USA
[b] DTU Chemical Engineering, Technical University of Denmark, DK-2800 Lyngby, Denmark
[c] Combustion Research Facility, Sandia National Laboratories, P.O. Box 969, Livermore, CA 94551-0969, USA

ARTICLE INFO

Article history:
Received 15 October 2010
Received in revised form 7 December 2010
Accepted 7 December 2010
Available online 13 January 2011

Keywords:
Ab initio calculations
Master equation
Chemical kinetics
Nitrogen chemistry
NNH
Thermal DeNO$_x$

ABSTRACT

One of the remaining issues in our understanding of nitrogen chemistry in combustion is the chemistry of NNH. This species is known as a key intermediate in Thermal DeNO$_x$, where NH_3 is used as a reducing agent for selective non-catalytic reduction of NO. In addition, NNH has been proposed to facilitate formation of NO from thermal fixation of molecular nitrogen through the so-called NNH mechanism. The importance of NNH for formation and reduction of NO depends on its thermal stability and its major consumption channels. In the present work, we study reactions on the NNH + O, NNH + O_2, and NH_2 + O_2 potential energy surfaces using methods previously developed by Miller, Klippenstein, Harding, and their co-workers. Their impact on Thermal DeNO$_x$ and the NNH mechanism for NO formation is investigated in detail.

1. Introduction

Emission of oxides of nitrogen from combustion and high temperature industrial processes continues to be a major environmental concern. Nitrogen oxides, collectively termed NO$_x$, are formed either from fixation of N_2 in the combustion air at high temperatures or from oxidation of nitrogen chemically bound in the fuel [1,2]. The concern about NO$_x$ emissions and the need to comply with increasingly stringent regulations have motivated a vast amount of research. Despite these efforts, there are still unresolved issues in formation and in situ control of nitrogen oxides.

One of the remaining issues in our understanding of nitrogen chemistry is the chemistry of NNH. This radical was first suggested as being important by Miller et al. [3], who considered it as a possible product of the NH_2 + NO reaction. Subsequent work, e.g. [4–19], has confirmed that NNH (or N_2 + H) is indeed formed in the NH_2 + NO reaction, and modeling studies have identified it as a key intermediate in Thermal DeNO$_x$ [9,19–23], where NH_3 is used as a reducing agent for selective non-catalytic reduction of NO.

More recently, NNH was proposed by Bozzelli and Dean [24] to facilitate formation of NO from thermal fixation of molecular nitrogen through the so-called NNH mechanism. The importance of NNH for formation and reduction of NO depends on its thermal stability and its major consumption channels. NNH is a free radical that dissociates exothermically into N_2 + H by tunneling through a small (<8 kcal mol^{-1}) potential energy barrier. The lifetime of NNH has been inferred from experiment to have an upper limit of 0.5 μs [25], but theoretical work (see [26] and discussion below) indicates values of 10^{-8}–10^{-11} s. Such a short lifetime implies that the N_2 + H recombination reaction is fast enough to maintain a partial equilibrium with NNH at combustion conditions. A subsequent reaction NNH + O = NH + NO then offers a high temperature pathway for NO formation, the so-called NNH mechanism. A number of experimental and modeling studies [27–32] support the existence of the NNH mechanism, and kinetic modeling indicates that it is of importance in premixed and non-premixed flames of both hydrogen [33–36] and hydrocarbons [37–42].

In the present work, we evaluate the thermochemistry and reactions of NNH. Specifically, we study reactions on the NNH + O, NNH + O_2, and NH_2 + O_2 potential energy surfaces using methods previously developed by Miller and Klippenstein [43–48] and Klippenstein and Harding [49–51]. Most importantly, we discuss their impact on Thermal DeNO$_x$ and the NNH mechanism for NO formation.

2. Theory

In order to say anything definitive about Thermal DeNO$_x$ or the NNH mechanism for NO formation, we must evaluate the thermochemistry and reactions of NNH. The heat of formation and the lifetime of NNH are discussed based on a review of the literature. We study the NNH + O and NNH + O_2 reaction systems using methods previously developed by Miller, Klippenstein, and Harding. In addi-

* Corresponding author.
E-mail address: pgl@kt.dtu.dk (P. Glarborg).

0010-2180/$ - see front matter © 2011 The Combustion Institute. Published by Elsevier Inc. All rights reserved.
doi:10.1016/j.combustflame.2010.12.013

tion, the $NH_2 + O_2$ reaction is analysed. These analyses are based on coupled-cluster (CCSD(T) and QCISD(T)) and multireference CASPT2 and CAS + 1 + 2 + QC electronic structure calculations, all of which were performed with the MOLPRO electronic structure package [52]. Structures and vibrational frequencies for the various structures considered here are provided in the supplementary material.

2.1. Heat of formation of NNH

As discussed more extensively below, the electronic structure of NNH has been studied numerous times since the early work of Miller and co-workers. Among these investigations the very recent work of Bozkaya et al. [26] appears to have the best calculation for the NNH ⇄ N_2 + H energy. An energy diagram based on their work is shown in Fig. 1. Including zero-point energies they give −8.8 kcal mol^{-1} for the dissociation energy. Taking the heat of formation of H atom at 0 K to be 51.6 kcal mol^{-1}, this dissociation energy gives an H_f(0 K) for NNH of 60.4 kcal mol^{-1}. Subtracting 0.7 kcal mol^{-1} for conversion to 298 K gives 59.7 kcal mol^{-1}. We employ this result in all the modeling results presented below.

2.2. Lifetime of NNH

The lifetime of NNH has been the subject of a number of theoretical studies [26,53–66]. Predictions for the ground state lifetime (τ_0) range from 3×10^{-11} to 4×10^{-8} s. Meanwhile, the excited vibrational states have lifetimes that are generally about three orders of magnitude shorter. Because of the vast difference in the lifetimes between the ground and excited vibrational states, we anticipate that a rigorous theoretical analysis would show a fairly broad regime of temperature and pressure where the steady-state population distribution during dissociation has significant population only in the ground state, resulting in a thermal dissociation rate coefficient that can be approximated accurately as the tunneling rate coefficient in this state. Of course, at temperatures and pressures where the excited states can be populated effectively from the ground state by collisions the rate coefficient will change, resulting in a dependence on temperature and pressure. However, the calculated lifetimes for the excited states suggest that pressures of the order of 100–1000 atmospheres would be required for this effect to be significant. Any excited NNH formed directly from the NH_2 + NO reaction would show up on the phenomenological time scale as contributing to the reaction $NH_2 + NO \rightarrow N_2 +$ H + OH reaction in the regime of interest. At least at lower temperatures experiments indicate that this latter reaction is not significant. A problem with our argument is that, because of the very short lifetimes involved, NNH dissociation may not yield to a rate-coefficient (phenomenological) description at all. Nevertheless, the lifetime used in a model should not be longer than the ground-state lifetime (it represents an upper limit) and under the present conditions, should be roughly of that magnitude. We cannot make any more precise statements about the thermal dissociation of NNH (or even verify our picture of it) without performing a fairly sophisticated theoretical analysis. This exercise must be left for another time.

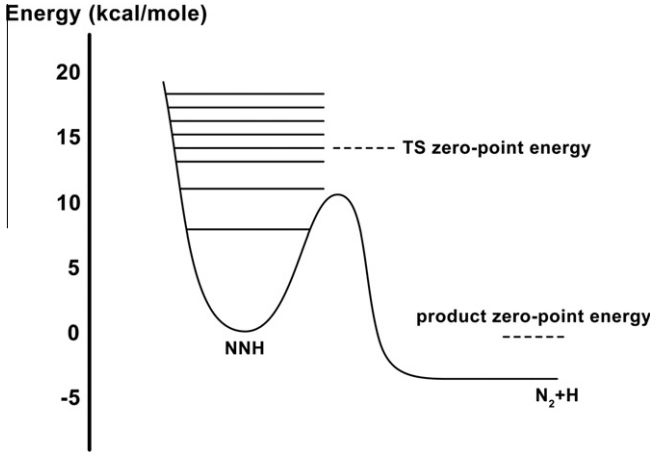

Fig. 1. Potential energy diagram for the NNH dissociation reaction. Also shown on the diagram are the lowest vibrational energy levels of the NNH molecule. The diagram is based on the theoretical work of Boskaya et al. [26].

The most recent study, by Bozkaya et al. [26], yields the longest predicted τ_0 of 3.6×10^{-8} s. The underlying electronic structure calculations in this study are the most extensive to date and yield a classical barrier height of 10.6 ± 0.2 kcal mol^{-1}. However, the lifetime is obtained from simple one-dimensional asymmetric Eckart tunneling calculations, which are not expected to be particularly accurate in this case. Indeed, errors exceeding an order of magnitude would not be unusual.

Earlier full-dimensional quantum dynamics calculations by Koizumi, Schatz, and Walch [56] (KSW) predicted a ground state lifetime of 3×10^{-9} s. Related calculations by Li and Guo [59] employing the same KSW potential, but with different dynamical methods, yielded an essentially identical ground state lifetime. Unfortunately, the classical barrier height of 11.4 kcal mol^{-1} for the KSW potential is significantly greater than the value determined by Bozkaya et al. Notably, the sample calculations of Koizumi et al. for a second surface with a classical barrier height of 10.5 kcal mol^{-1} yield a predicted τ_0 that is within a factor of 5 of their main prediction.

More recently, Caridade et al. [63] have used full-dimensional quantum dynamics calculations to predict a ground state lifetime of 4×10^{-10} s for a new more accurate potential energy surface. However, their predictions for the KSW potential differ by a factor of two from the earlier calculations of Koizumi et al. and of Li and Guo. Furthermore, their calculations for the KSW potential have a stated uncertainty of nine times the predicted value. Although not reported, their uncertainties for their reference potential are presumably of similar magnitude.

Taken together, the Koizumi et al. and Caridade et al. calculations suggest that the best estimate for τ_0 is approximately 8×10^{-10} s, which correlates with a decrease in the KSW value by a factor of 4 due to the overestimated barrier height. It also correlates with a factor of 2 increase in the Caridade et al. estimate in response to apparent errors in their dynamics methods. Importantly, this estimate is for tunneling from the ground rotational state. Guo and Thompson [61] have performed an interesting semiclassical study of the effect of rotation on the lifetime. Their calculations suggest that the lifetime increases by a factor of 2.4 for a rotational energy of 5 kcal mol^{-1}. Including such a rotational correction implies a best estimate for the lifetime of thermal rotational states of NNH at 1000–1500 K of 1 or 2×10^{-9} s. Unfortunately, the uncertainty in this prediction is still significant. Ideally, the lifetimes for explicit rotational states of NNH would be calculated for a highly accurate potential energy surface, such as the one recently presented by Motas and Varandas [66]. We have adopted a value of $\tau_0 = 10^{-9}$ s in the modeling discussed below.

2.3. NNH + O_2

There do not appear to be any prior experimental or *ab initio* theoretical studies of the NNH + O_2 reaction, although Dean and Bozzelli [67] applied qualitative QRRK concepts to estimate the rates and branching for this reaction. The radical character of the

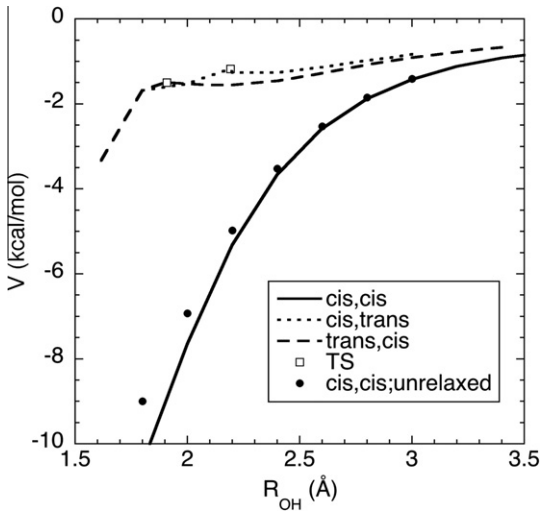

Fig. 2. Plot of the CASPT2(11e,9o)/aug-cc-pVDZ minimum energy path potential for the cis,cis; cis,trans; and trans,cis abstraction pathways in NNH + O_2, where the first cis/trans designation denotes the OHNN dihedral angle and the second denotes the OOHN angle. The open squares denotes the saddle points for the cis,trans and trans,cis reaction. The solid circles denote the cis,cis MEP obtained when the NNH and O_2 structures are held fixed at their separated fragment values.

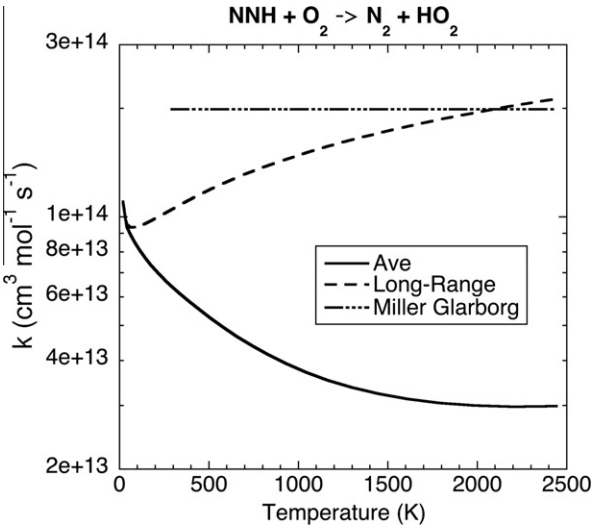

Fig. 3. Plot of the temperature dependence of the rate coefficient for the NNH + O_2 abstraction reaction. The solid line denotes the present dynamically corrected direct CASPT2 VRC-TST predictions, the dashed line denotes the predictions when restricting the TS to long range, and the dash–dot–dot–dot line denotes the values employed in our prior modeling studies [22].

NNH and O_2 species suggests that the NNH + O_2 reaction might involve the formation of an OONNH complex, as Dean and Bozzelli presume. However, this complex is endothermic relative to reactants, and so no complex formation is predicted here. Instead, the reaction of NNH with O_2 involves a barrierless abstraction to form the highly exothermic products N_2 + HO_2 (−57 kcal mol^{-1}).

The abstraction minimum-energy paths (MEPs) are illustrated in Fig. 2 for various torsional states. These MEPs are obtained from constrained optimizations with multi-reference second-order perturbation theory CASPT2 [68,69] employing the aug-cc-pVDZ basis set [70]. The active orbitals in the 11-electron, 9-orbital (11e,9o) CAS part of this calculation correlate with the radical orbital of NNH (1e,1o), the NH σ, σ^* orbitals (2e,2o), and the π spaces of NNH (2e,2o) and O_2 (6e,4o). The cis,cis abstraction pathway, which involves the partial formation of a five-membered OOHNN ring, is clearly the dominant pathway. The cis,trans and trans,cis pathways are also essentially barrierless, with the latter involving the partial formation of a four-membered OOHN ring. The trans,trans path was also explored, but it was found to relax to the cis,cis path at OH separations of 2.4 Å and smaller.

Also included in Fig. 2 is a plot of the MEP obtained when optimizing only the OHN and OOH angles. The small difference between the full MEP and this partially optimized MEP suggests that the variable-reaction-coordinate transition-state theory (VRC-TST) approach [71,72] is directly applicable to this abstraction reaction. Here we implement this approach with direct CASPT2(7e,5o) calculations employing both the cc-pVDZ and aug-cc-pVDZ basis sets. The final estimates are obtained from the average for these two basis sets. The maximum discrepancy between the two is ∼50%. The (7e,5o) active space consists of the radical orbital of NNH and the (6e,4o) π space of O_2.

The VRC-TST calculations include one-dimensional corrections for limitations in the basis set, for larger active spaces, and for the effects of geometry relaxation, each of which is obtained from consideration of the cis,cis MEP. The basis-set corrections are obtained from the average of CBS estimates based on the extrapolation of cc-pVnZ or aug-cc-pVnZ calculations, where n = T and Q for both cases. The active-space correction is given by the difference between CASPT2(11e,9o)/aug-cc-pVDZ and CASPT2(7e,5o)/aug-cc-pVDZ results. The geometry relaxation correction is obtained from the difference of the full and partially optimized MEPs (cf. Fig. 2). The reaction-coordinate and dividing-surface optimizations consider both a fixed center-of-mass separation and a fixed OH separation, each for a range of distances.

The present direct CASPT2-based VRC-TST predictions for the NNH + O_2 → N_2 + HO_2 rate coefficient are illustrated in Fig. 3. The predictions include a dynamical correction factor of 0.85 as evaluated for related radical–radical reactions [49]. These predictions are estimated to have an overall uncertainty of a factor of 1.5. The modified Arrhenius expression $5.55 \times 10^{13} T^{-0.385}$ exp(13.4/RT) cm^3 mol^{-1} s^{-1} provides a satisfactory reproduction of these results over the 200–2400 K temperature range.

Figure 3 also illustrates the results of a calculation in which the transition-state dividing surfaces are restricted to long-range, i.e., 4.5 Å and greater. This long-range result approximates the collision limit and provides an upper bound to the true rate coefficient. The much smaller values for the full VRC-TST calculations indicate that there are significant entropic bottlenecks to the abstraction that arise at short-range. Near 1000 K the full VRC-TST predictions are about a factor of 5 lower than the rate coefficient employed in our previous modeling studies [21,22], where it was assumed that the rate coefficient would be close to the collision limit.

Notably, Dean and Bozzelli [67] predict a rate coefficient of $\sim 10^{11}$ cm^3 mol^{-1} s^{-1}, which is two orders of magnitude smaller than the present predictions. They also predict 20% branching to OH + N_2O. Our own limited B3LYP density-functional-theory search for a pathway leading to these products suggests that the latter branching is negligible.

Under conditions with a large concentration of O_2, the reaction of NNH with O_2 could conceivably provide an alternative route to the formation of NO through an HNO + NO channel. However, limited B3LYP calculations suggest a very high barrier of about 58 kcal mol^{-1} for this channel, which effectively negates any possible contribution from it.

2.4. NNH + O

The reaction of NNH with O has been the subject of a recent high-level theoretical study [32]. Here, we build on this work, making improvements to a number of key aspects. Most importantly,

we employ VRC-TST and trajectory simulations on potential energy surfaces based on multireference electronic-structure theory to obtain more accurate estimates of the entrance channel and NH + NO transition-state fluxes. We also make a number of corrections to the energies and pathways in the underlying potential energy surface for subsequent isomerizations and dissociations. These corrections are incorporated in our master equation for the overall kinetics.

The potential energy surface for the interaction of NNH with O is remarkably attractive (cf. Fig. 4). There are barrierless reaction paths for addition to the terminal N from both the cis and trans side, for addition to the central N atom from the trans side, and for abstraction of the H atom. An analytic representation of this interaction potential was obtained here via a fit to a set of Davidson-corrected multireference singles and doubles configuration interaction calculations (CAS + 1 + 2 + QC). The (7e,6o) active space for these calculations consists of the (4e,3o) p space of O, the radical orbital of NNH, and the (2e,2o) π space of NNH. These calculations employed an aug-cc-pVDZ basis set and the CAS part of the calculation averaged over the three states correlating with the nearly degenerate states of O(^{3}P). Analytic potentials were obtained for both the ground and first excited states, both of which are attractive. The third state is repulsive at short separation and so does not contribute to the kinetics.

We have evaluated the total rate coefficient and branching fractions for the four different channels with both trajectory simulations and VRC-TST calculations. The branching ratio estimates require approximate dividing surfaces for delineating the different channels. This separation is somewhat imprecise due to the attractiveness at all orientations. Nevertheless, the predictions are reasonably insensitive to modest variations in the divisions between the channels. The predicted overall rate coefficient from the trajectory calculations is ~0.89 times that from the VRC-TST estimates. The branching fractions predicted by the two methods are also quite similar. The contributions to the rate coefficients from the first excited state are typically about 85% of those from the ground state.

For computational reasons, the final master-equation analysis for the channel-specific bimolecular rate coefficients employs adjusted VRC-TST predictions for the individual fluxes. These adjustments involve a reduction in the rate coefficients for the cis and trans additions; the corrections involve multiplicative factors of 0.8 and 0.7, respectively. These reductions yield a total rate coefficient and branching ratios that reasonably reproduce the more limited trajectory values.

The potential energy surface for the subsequent isomerizations and dissociations in the reaction of NNH with O was studied here with electronic-structure methods that are closely related to those employed by Haworth et al. [32]. A schematic plot of this potential is provided in Fig. 5 and the stationary-point energies are reported in Table 1. The rovibrational properties and zero-point energies were analyzed with the B3LYP/6–311++G(d,p) density functional method. The primary energies come from RQCISD(T)/CBS calculations with the CBS extrapolation given by the average of extrapolations based on either cc-pVnZ or aug-cc-pVnZ basis sets, with n = Q,5. The two extrapolations typically agreed to within a few tenths of a kcal mol^{-1}, and the extrapolation generally predicted a difference from n = 5 results of 0.6 kcal mol^{-1} or less. Core-valence correlation corrections (0.4 kcal mol^{-1} or less) were evaluated from CBS extrapolations of aug-cc-pCVnZ calculations, with n = T,Q. Relativistic corrections (0.3 kcal mol^{-1} or less) were obtained from CAS calculations with the aug-pCVTZ basis set.

Related results for the stationary-point energies from Haworth et al. [32] are also reported in Table 1. The predicted energies are remarkably different for a number of species. In many instances the two calculations differ by more than their stated maximum uncertainty of 1.0 kcal mol^{-1}. An attempt to reproduce their results indicates some error in their CCSD(T)/aug-cc-pV5Z energies, which gets magnified in their basis-set extrapolation. For comparison we report our own RCCSD(T)/CBS results including corrections, which should be closely comparable to their results. Another more minor

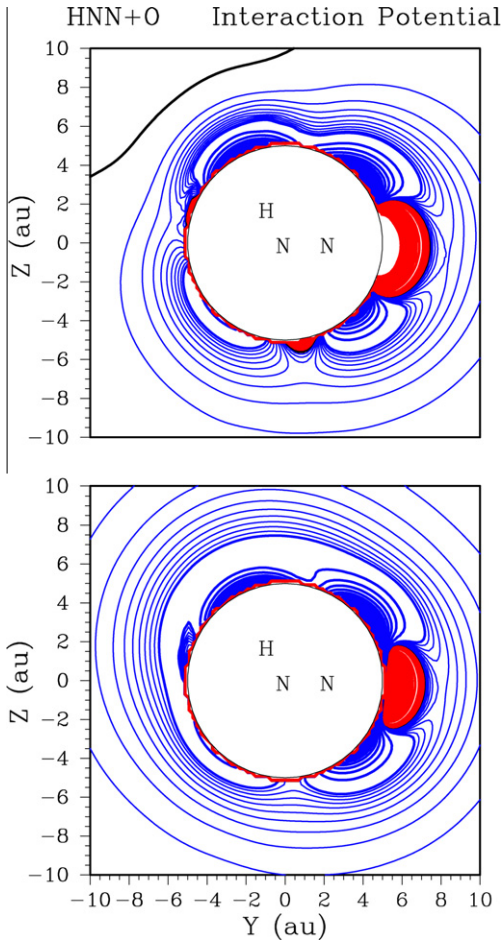

Fig. 4. Potential energy contours for O + NNH in the ground (lower) and first excited (upper) states. Blue contours denote attractive regions, red denote repulsive regions. The contour increment for the thin contours is 0.1 kcal/mol. The increment for the thick contours is 1.0 kcal/mol. (For interpretation of the references to colours in this figure legend, the reader is referred to the web version of this paper.)

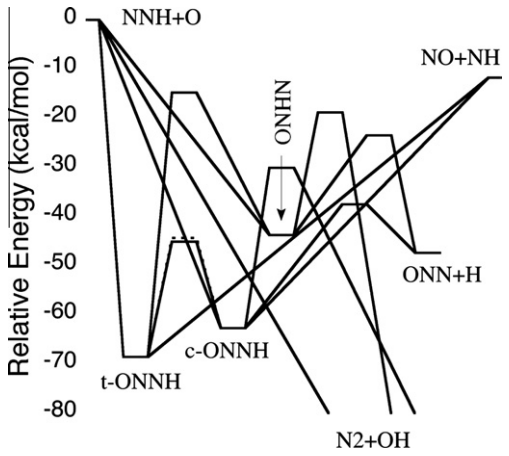

Fig. 5. Schematic plot of the potential energy surface for the reaction of NNH with O atoms. The dashed line above the t-ONNH to c-ONNH transition state denotes the excited state transition state.

Table 1
Energies on the NNH + O potential energy surface relative to NNH + O.[a]

Species	RQCISD(T)/ CBS{Q,5}[b]	UCCSD(T)/CBS{Q,5}[b]	RCCSD(T)/CBS{Q,5}[b]	RCCSD(T)/CBS{Q,5}[c]	G3X[c]	T1 Diag.
N_2 + OH	−110.36	−110.16	−110.54	−110.5	−111.0	0.013, 0.008
NNO + H	−47.43	−46.49	−46.98	−46.7	−48.3	0.021
NH + NO	−11.73	−11.58	−11.66	−11.3	−14.1	0.021, 0.006
trans-ONNH	−68.60	−67.98	−67.67	−69.9	−69.0	0.035
cis-ONNH	−62.77	−62.10	−62.16	−63.9	−62.7	0.026
ONHN	−43.78	−43.23	−43.36	−46.9	−44.7	0.024
trans-ONNH <-> cis-ONNH; torsion	−45.15	−44.95	−43.85		−46.2	0.054
trans-ONNH <-> cis-ONNH; bend	−44.37	−41.34	−41.40			0.024
trans-ONNH <-> ONHN	−14.82	−14.17	−13.78	−13.8	−15.4	0.037
cis-ONNH <-> ONN + H	−37.53	−36.84	−36.94	−39.6	−38.7	0.024
cis-ONNH <-> N_2 + OH	−30.08	−29.67	−28.78	−29.3	−29.2	0.046
ONHN <-> ONN + H	−23.50	−22.75	−22.72	−25.3	−24.3	0.025
ONHN <-> N_2 + OH	−18.84	−18.12	−16.85	−17.7	−18.7	0.054

[a] Energies in kcal/mol.
[b] Present work, including zero-point energy, core-valence, spin–orbit, and relativistic corrections.
[c] From Ref. [32].

discrepancy involves the relativistic corrections, with theirs being larger by about a factor of 2.

A final distinction between the two calculations arises from our preference for the RQCISD(T) method. From our experience, the RQCISD(T) method provides energy estimates that are similar to the UCCSD(T) method, both of which are more accurate than the RCCSD(T) method. Table 2 includes the results from each of these methods. There are clearly some significant differences between them for this system. The differences between the RCCSD(T) and UCCSD(T) results are greatest for the cases with large T1 diagnostics, which is taken to be an indicator of multireference effects. The differences between the RQCISD(T) and UCCSD(T) results are harder to understand and provide some indication of the level of uncertainty in the PES.

Fortunately, the two transition states with large T1 diagnostics have little bearing on the rate-coefficient predictions. The torsional transition state for isomerization from trans-ONNH to cis-ONNH is low enough in energy that isomerization is expected to be rapid even with a moderate change in its energy. Furthermore, there is a low-energy bending transition state that also serves to rapidly equilibrate the cis–trans isomers. The transition state for decomposition to N_2 + OH from ONHN has little effect on the predicted branching to N_2 + OH from NNH + O because the direct abstraction provides the dominant pathway to these products. Thus, we have chosen not to perform any multireference evaluations for these two transition states with high T1 diagnostics.

The collisionless-limit rate coefficients were evaluated from master-equation calculations employing transition-state-theory estimates for each of the channels illustrated in the schematic PES (cf. Fig. 5). The partition functions for the transition states with well defined saddle points were obtained from rigid-rotor, harmonic-oscillator estimates, including hindered-rotor corrections as appropriate. Those for the barrierless entrance channels were obtained from the combination of VRC-TST and trajectory calculations, as described above. The barrierless NH + NO channel was also treated with VRC-TST as described below. The calculations indicate essentially no pressure dependence for realistic ranges of pressure. Indeed, the total association rate coefficient is within 20% of the collisionless-limit rate coefficient for temperatures up to 2000 K.

The present predictions for the overall and channel-specific rate coefficients are illustrated in Fig. 6. The predictions are similar to those of Haworth et al., although the two sets of predictions differ by as much as a factor of 3. The primary products are predicted to be N_2 + OH, with significant branching to N_2O + H. The endothermicity of the NO + NH channel makes this a relatively minor channel even at 2000 K. The calculated rate coefficients are reproduced well by the modified Arrhenius expressions: $k_{N_2+OH} = 1.20 \times 10^{13} T^{0.145} \exp(217/RT)$, $k_{NNO+H} = 1.87 \times 10^{14} T^{-0.274} \exp(21.7/RT)$, and $k_{NH+NO} = 5.18 \times 10^{11} T^{0.388} \exp(409/RT)$ cm^3 mol^{-1} s^{-1} over the 300–2500 K temperature range. The predicted rate coefficients for each of these channels are estimated to have an uncertainty of a factor of 2.

2.5. NH + NO

The NNH + O potential energy surface also allows us to examine the kinetics of the NH + NO and H + N_2O reactions. The entrance channel for the NH + NO reaction is barrierless, and so again we apply direct VRC-TST to this channel. In this case, the orientation-dependent interaction energies were obtained from CASPT2 (7e,6o)/aug-cc-pVDZ calculations. A one-dimensional correction for geometry relaxation was obtained with the same method, while a correction for limitations in the basis set was obtained from an average of cc-pVnZ- and aug-cc-pVnZ-based CBS extrapolations with n = T,Q. The active space in these CAS calculations consisted of the two radical orbitals in ^{3}NH and the (5e,4o) π-space of NO. The CAS wavefunction is for an average of the two states correlating with the doubly degenerate ground state of NO.

The contributions from both the ground state, correlating with the 2A′ state in Cs symmetry, and the first excited state, correlating with the 2A″ state, were included in the VRC-TST analysis. The first excited state was found to make a negligible contribution for temperatures up to 3000 K. Similarly, a quartet pathway was explored and found to be insignificant.

The VRC-TST analysis included an approximate separation into cis and trans addition products. Pivot points were placed at a grid of locations along the internuclear axis for both NH and NO.

The present *ab initio* TST based predictions for the NH + NO rate coefficients are plotted in Fig. 7. Again little pressure dependence is expected, and so we consider only the collisionless-limit rate coefficients. This reaction has been studied extensively in the laboratory. For simplicity, we restrict our comparison to the recent review of Baulch et al. [73], which suggests that the literature rate

Table 2
Selected reactions in the H/N/O subset. Units are cm, mol, s, cal.

		A	*n*	*E*	
1	$NH_3 + M = NH_2 + H + M$	2.2E16	0.000	93,470	[92]
2	$NH_3 + H = NH_2 + H_2$	6.4E05	2.390	10,171	[92]
3	$NH_3 + O = NH_2 + OH$	2.8E02	3.290	4471	[96]
4	$NH_3 + OH = NH_2 + H_2O$	2.0E06	2.040	566	[92]
5	$NH_3 + HO_2 = NH_2 + H_2O_2$	3.0E11	0.000	22,000	[92]
6	$NH_2 + H = NH + H_2$	7.2E05	2.320	799	[92]
7	$NH_2 + O = HNO + H$	6.6E13	0.000	0	[94]
8	$NH_2 + O = NH + OH$	7.0E12	0.000	0	[94]
	$NH_2 + O = NH + OH$	8.6E−1	4.010	1673	
	Duplicate reaction				
9	$NH_2 + OH = NH + H_2O$	3.3E06	1.949	−217	[96], [a]
10	$NH_2 + HO_2 = H_2NO + OH$	5.0E13	0.000	0	[92]
11	$NH_2 + HO_2 = NH_3 + O_2$	9.2E05	1.940	−1152	[92]
12	$NH_2 + O_2 = H_2NO + O$	2.6E11	0.4872	29,050	pw
13	$NH_2 + O_2 = HNO + OH$	2.9E−2	3.764	18,185	pw
14	$NH_2 + NO = N_2 + H_2O$	1.3E16	−1.250	0	See text, [b]
	$NH_2 + NO = N_2 + H_2O$	−3.1E13	−0.480	1180	
	Duplicate reaction				
15	$NH_2 + NO = NNH + OH$	3.1E13	−0.480	1180	See text, [b]
16	$NH_2 + HNO = NH_3 + NO$	3.6E06	1.630	−1250	[92]
17	$NH_2 + NO_2 = N_2O + H_2O$	3.0E14	−0.770	242	[98]
18	$NH_2 + NO_2 = H_2NO + NO$	1.3E15	−0.770	242	[98]
19	$NH_2 + HONO = NH_3 + NO_2$	7.1E01	3.020	−4940	[92]
20	$NH + H = N + H_2$	3.0E13	0.000	0	[92]
21	$NH + O = NO + H$	9.2E13	0.000	0	[92]
22	$NH + OH = HNO + H$	3.2E14	−0.376	−46	[96]
23	$NH + OH = N + H_2O$	1.6E07	1.733	−576	[96]
24	$NH + O_2 = HNO + O$	4.6E05	2.000	6500	[92]
25	$NH + O_2 = NO + OH$	1.3E06	1.500	100	[92]
26	$NH + NO = N_2O + H$	1.8E14	−0.351	−244	pw
27	$NH + NO = N_2 + OH$	2.7E12	−0.0721	−512	pw
28	$NH + NO_2 = HNO + NO$	5.9E12	0.000	0	[101,102]
29	$NH + NO_2 = N_2O + OH$	4.1E12	0.000	0	[101,102]
30	$N + OH = NO + H$	3.8E13	0.000	0	[92]
31	$N + O_2 = NO + O$	6.4E09	1.000	6280	[92]
32	$N + NO = N_2 + O$	2.1E13	0.000	0	[94]
33	$NNH = N_2 + H$	1.0E09	0.000	0	See text
34	$NNH + H = N_2 + H_2$	1.0E14	0.000	0	[92]
35	$NNH + O = N_2O + H$	1.9E14	−0.274	−22	pw
36	$NNH + O = N_2 + OH$	1.2E13	0.145	−217	pw
37	$NNH + O = NH + NO$	5.2E11	0.388	−409	pw
38	$NNH + OH = N_2 + H_2O$	5.0E13	0.000	0	[92]
39	$NNH + O_2 = N_2 + HO_2$	5.6E14	−0.385	−13	pw
40	$NNH + NO = N_2 + HNO$	5.0E13	0.000	0	[92]
41	$NO + H(+ M) = HNO(+M)$	1.5E15	−0.410	0	[92]
	Low pressure limit	2.4E14	0.206	−1550	
	Troe parameters 0.82 1E−30 1E30				
	Third body efficiencies: $N_2 = 1.6$				
42	$HNO + H = NO + H_2$	4.4E11	0.720	650	[92]
43	$HNO + O = NO + OH$	2.3E13	0.000	0	[92]
44	$HNO + OH = NO + H_2O$	3.6E13	0.000	0	[92]
45	$HNO + O_2 = NO + HO_2$	2.0E13	0.000	16,000	[92]
46	$H_2NO + M = HNO + H + M$	2.8E24	−2.830	64,915	[92]
	Third body efficiencies: $H_2O = 10$				
47	$H_2NO + H = HNO + H_2$	3.0E07	2.000	2000	[92]
48	$H_2NO + H = NH_2 + OH$	5.0E13	0.000	0	[92]
49	$H_2NO + O = HNO + OH$	3.0E07	2.000	2000	[92]
50	$H_2NO + OH = HNO + H_2O$	2.0E07	2.000	1000	[92]
51	$H_2NO + HO_2 = HNO + H_2O_2$	2.9E04	2.690	−1600	[92]
52	$H_2NO + O_2 = HNO + HO_2$	3.0E12	0.000	25,000	[92]
53	$NO + O(+M) = NO_2(+M)$	1.3E15	−0.750	0	[92]
	Low pressure limit	4.7E24	−2.870	1550	
	Troe parameters 0.88 1E03 1E04 1E30				
54	$NO + HO_2 = NO_2 + OH$	2.1E12	0.000	−497	[92]
55	$NO_2 + H = NO + OH$	1.3E14	0.000	362	[92]
56	$NO_2 + O = NO + O_2$	1.1E14	−0.520	0	[93]
57	$NO_2 + HO_2 = HONO + O_2$	1.9E00	3.320	3044	[93]
58	$NO_2 + HO_2 = HNO_2 + O_2$	1.9E01	3.260	4983	[93]
59	$N_2O(+M) = N_2 + O(+M)$	1.3E12	0.000	62,570	[92]
	Low pressure limit	4.0E14	0.000	56,600	
60	$N_2O + H = N_2 + OH$	6.4E07	1.835	13,492	pw
61	$N_2O + O = NO + NO$	9.2E13	0.000	27,679	[92]
62	$N_2O + O = N_2 + O_2$	3.7E12	0.000	15,936	[92]

(*continued on next page*)

Table 2 (*continued*)

		A	*n*	*E*	
63	$N_2O + OH = N_2 + HO_2$	1.3E−2	4.720	36,560	[92]
64	$N_2O + OH = HNO + NO$	1.2E−4	4.330	25,080	[92]

[a] k_9 is the theoretical value derived by Klippenstein et al. [96], before adjusting the barrier height to obtain a better agreement with shock tube data.
[b] the rate coefficients are fitted in the temperature range 700–2500 K.

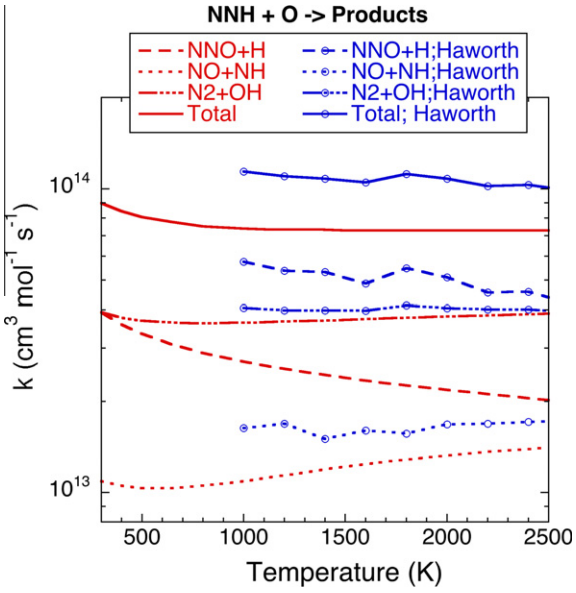

Fig. 6. Plot of the collisionless-limit rate coefficients for NNH + O. The red lines denote the present *ab initio* TST based predictions, while the blue lines with open circles denote the computational results from Haworth et al. [32]. (For interpretation of the references to colour in this figure legend, the reader is referred to the web version of this article.)

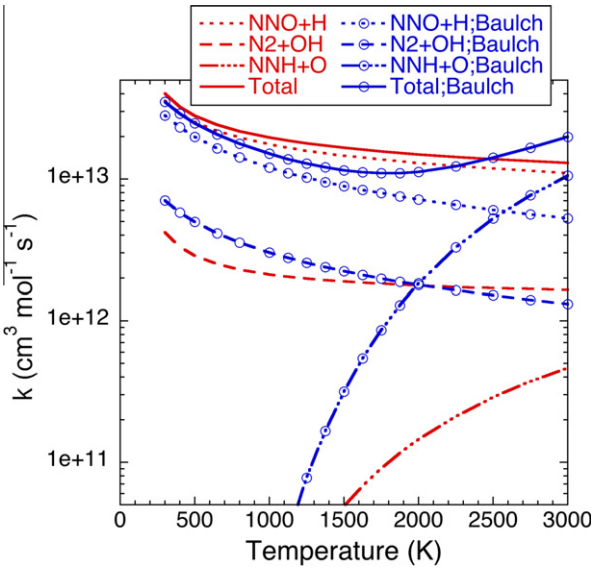

Fig. 7. Plot of the collisionless-limit rate coefficients for NH reacting with NO. The red lines denote the present *ab initio* TST based predictions, while the blue lines with open circles denote the review of Baulch et al. [73]. (For interpretation of the references to colour in this figure legend, the reader is referred to the web version of this article.)

coefficients have an uncertainty of a factor of 2. Overall, the present predictions are in good agreement with this review, with a maximum discrepancy between the two total rate constants of less than a factor of 1.5. However, our *ab initio* based predictions suggest a shallower decay with temperature in the 1000–2000 K region and no rise at higher temperatures. The absence of a rise at higher temperature correlates with a lower predicted rate coefficient for the NNH + O channel. Baulch et al. use a larger high-temperature rate coefficient for this channel to explain the experimentally observed rise in the total rate constant. The present predictions for the channel-specific rate coefficients are reproduced well by the modified Arrhenius expressions $k_{NNO+H} = 1.75 \times 10^{14} T^{-0.351}$ exp(244/RT), $k_{N_2+OH} = 2.69 \times 10^{12} T^{-0.0721}$ exp(513/RT), and $k_{NNH+O} = 1.94 \times 10^{10} T^{0.624}$ exp(−10,870/RT) cm^3 mol^{-1} s^{-1} over the 500–3000 K temperature range. We estimate the uncertainty in our prediction of the total rate coefficient to be a factor of 1.3.

2.6. $H + N_2O$

The last reaction we want to use to test our potential for the ONNH system is that between nitrous oxide and hydrogen atoms. This reaction has been studied a number of times in the laboratory, but the 1987 paper of Marshall et al. [74] appears to be the most accurate and comprehensive investigation to date. These authors measured the total rate coefficient between 390 K and 1310 K. There appears to be little or no disagreement in the literature about the products – the consensus is that the reaction produces N_2 + OH exclusively under conditions of interest.

The master-equation analysis employed an exponential-down energy transfer model with $\langle \Delta E_{down} \rangle = 100\ (T/300)^{0.85}$ cm^{-1}. This expression is typical of what we have found for small molecules interacting with weak colliders [75–85].

In Fig. 8 we compare our theoretical predictions of the rate coefficient with the results of Marshall et al. The agreement is remarkably good. The most interesting result of our analysis is that the "low-temperature curvature" in the Arrhenius plot is not due to tunneling, as suggested by Marshall et al. Instead, it is due to stabilization in the cis- and trans-HNNO wells at low temperatures. The bimolecular channels (N_2 + OH, NH + NO, and NNH + O) have

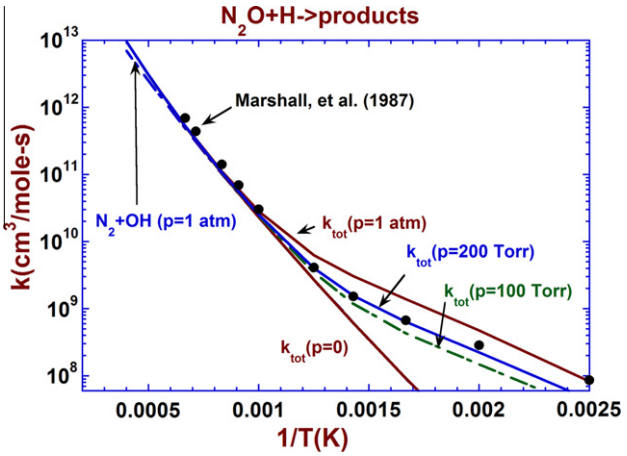

Fig. 8. Comparison of the theoretical predictions of k_{tot} for the N_2O + H reaction with the experiments of Marshall, Fontijn, and Melius [74]. The experiments involved a range of pressures (argon), with the median at slightly less than 200 torr.

rate coefficients that are essentially independent of pressure at least up to $p = 1$ atm. The most important of the three channels is, in fact, $N_2 + OH$, as indicated in the figure. The other channels only begin to come into play at high temperature where the $N_2 + OH$ curve begins to deviate from k_{tot}.

The collisionless-limit channel-specific rate coefficients are reproduced well by the modified Arrhenius expressions $k_{N_2+OH} = 6.44 \times 10^7\ T^{1.84}\ \exp(-13{,}490/RT)$, $k_{NO+NH} = 7.34 \times 10^{20} T^{-1.55} \exp(-36{,}940/RT)$, and $k_{NNH+O} = 2.25 \times 10^{19} T^{-1.10} \exp(-48{,}180/RT)$ $cm^3\ mol^{-1}\ s^{-1}$ over the 500 to 2500 K temperature range. The uncertainty in these predictions is about a factor of 2 near 1000 K.

2.7. $NH_2 + O_2$

Although the reaction of NH_2 with O_2 has been the subject of a few experimental studies, little is known about it other than that it is slow [86–89]. Nevertheless, this reaction has been reported to be of significance to the Thermal DeNO_x process at high concentrations of O_2 [21,22]. Building on earlier work of Melius and Binkley [90] and Sumathi and Peyerimhoff [91], we have evaluated the stationary-point energies in the $NH_2 + O_2$ reaction at the QCISD(T)/CBS{T,Q}//B3LYP/6–311++G(d,p) level.

A schematic plot of this potential energy surface is shown in Fig. 9. There are two product channels:

$$NH_2 + O_2 \rightarrow H_2NO + O \quad (R12)$$

$$NH_2 + O_2 \rightarrow HNO + OH \quad (R13)$$

The $H_2NO + O$ channel arises from a simple bond fission of the initial H_2NOO adduct, while the HNO + OH channel arises from isomerization via a tight 4-center transition state, leading to HNOOH, followed by decomposition of this complex to HNO + OH. The much lower entropy for the 4-center transition state coupled with its lower energy implies that the HNO + OH channel should be dominant at low temperature, while the $H_2NO + O$ channel should be dominant at high temperature. Due to the low stability of the H_2NOO complex no pressure dependence is expected at combustion temperatures.

We have used TST to make predictions for the temperature dependence of the rate coefficient for each of the channels. For HNO + OH we have employed rigid-rotor, harmonic-oscillator assumptions within tunneling corrected conventional TST. However, there is a large T1 diagnostic of 0.065 for the 4-center TS leading to HNOOH. Thus, we have also performed multireference CASPT2/CBS and CAS + 1 + 2 + QC/CBS calculations with both (3e,3o) and (7e,7o) actives spaces. The geometries and vibrational frequencies for these multireference calculations were obtained at the CASPT2(3e,3o)/cc-pVTZ level. The orbitals in this (3e,3o) active space correlate in H_2NOO with the radical orbital and the σ, σ^* orbitals of the active NH bond (or equivalently in HNOOH with the radical orbital and the σ, σ^* orbitals of OH). The (7e,7o) active space also includes the NO and OO σ, σ^* orbitals. The 4-center transition state is predicted to be 29.3, 34.8, 30.4, or 33.3 kcal mol^{-1} above the H_2NOO minimum for the CASPT2(3e,3o), CAS + 1 + 2 + QC(3e,3o), CASPT2(7e,7o), and CAS + 1 + 2 + QC(7e,7o) calculations, respectively. The (7e,7o) CASPT2 and CAS + 1 + 2 + QC barriers are 1.5 kcal mol^{-1} below and above the QCISD(T) results, respectively, suggesting the uncertainty in this barrier is ~2 kcal mol^{-1}.

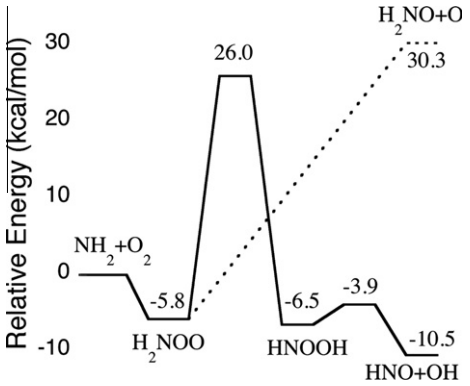

Fig. 9. Schematic plot of the potential energy surface for the reaction of NH_2 with O_2.

For the $H_2NO + O$ channel we have implemented direct CAS + 1 + 2 + QC VRC-TST. The $H_2NO + O$ reaction has many similarities to the NNH + O reaction. In particular, there are two strongly attractive doublet surfaces and one repulsive surface. In this case, the contribution from the first excited state is about ½ that from the ground state. There are also multiple reaction sites with barrierless attacks at the H's, the N, and the O. Here, we are only interested in the addition to form H_2NOO due to our focus on the $NH_2 + O_2$ reaction. With this in mind an approximate separation from the other channels is implemented. The orientation-dependent interaction energies for the VRC-TST calculations are evaluated at the CAS + 1 + 2 + QC(5e,4o)/aug-cc-pVDZ level. The CAS part is averaged over the three states correlating with the degenerate states of the O atom. Calculations at the CAS + 1 + 2 + QC(7e,5o) level were used to obtain one-dimensional geometry relaxation, active-space (both with the aug-cc-pVDZ basis), and basis-set corrections (with basis-set extrapolation of aug-cc-pVTZ and aug-cc-pVQZ calculations). A range of pivot points displaced above and below the O atom in H_2NO were considered in addition to center-of-mass pivot points.

One additional complication arises for the $H_2NO + O$ channel. In particular, H_2NO is slightly distorted from planarity, which implies that the umbrella mode should be highly anharmonic with a double well potential. At the B3LYP/6–311++G(d,p) level this mode has a frequency of only 89 cm^{-1}. In contrast, at the QCISD(T)/CBS{T,Q} level this mode has a frequency of 349 cm^{-1}. We have evaluated the angular potential for this mode at the QCISD(T)/cc-pVQZ level and used that to obtain an anharmonic correction for the partition function. Although the potential is highly anharmonic, the effect on the partition function of the double minimum and the restriction on angular ranges largely cancel. As a result, at least from room temperature to 2000 K, the anharmonic partition function differs by less than 20% from the corresponding harmonic one.

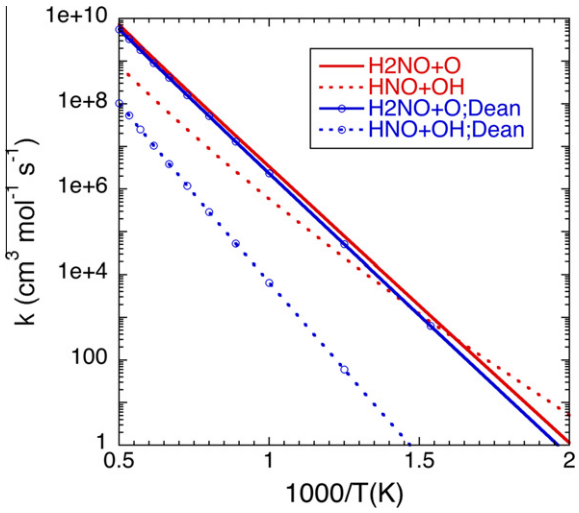

Fig. 10. Arrhenius plot of the channel-specific rate coefficients for the reaction of NH_2 with O_2. The red lines denote the present *ab initio* TST predictions while the blue lines with open circles denote the QRRK estimates from Dean and Bozzelli [67]. (For interpretation of the references to colour in this figure legend, the reader is referred to the web version of this article.)

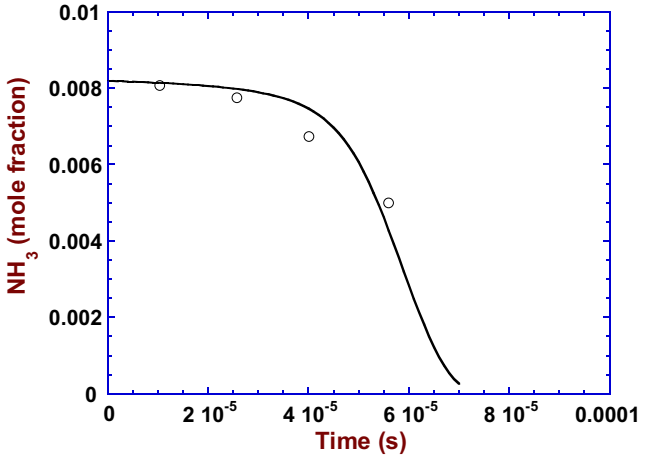

Fig. 11. Comparison of predictions of the present model with the experimental results of Fujii et al. [86] for NH_3 concentration as function of time in a reflected shock tube experiment at 5.1 atm and 2160 K. Inlet mole fractions: NH_3 = 0.0082, O_2 = 0.0082, balance Ar.

The present *ab initio* TST based predictions for the rate coefficients are illustrated in Fig. 10. These predictions are reproduced well by the modified Arrhenius expressions $k_{H_2NO+O} = 2.62 \times 10^{11} T^{0.487} \exp(-29{,}050/RT)$ and $k_{HNO+OH} = 2.88 \times 10^{-2} T^{3.76} \exp(-18{,}180/RT)$ $cm^3\ mol^{-1}\ s^{-1}$ over the 500–2500 K temperature range. Near 1000 K we estimate the uncertainty in our predictions to be factors of 2 and 4 for the $H_2NO + O$ and $HNO + OH$ channels, respectively. For temperatures of 600 K and higher, the $H_2NO + O$ channel is dominant. The earlier qualitative QRRK calculations of Dean and Bozzelli [67] yielded remarkably good estimates for the rate coefficient for this channel, as illustrated in Fig. 10. In contrast, their predictions for the HNO + OH channel are too small by one to two orders of magnitude.

In the absence of direct measurements for the $NH_2 + O_2$ rate coefficient, we have evaluated our calculated rate constant by comparing model predictions to global experimental data for NH_3 oxidation. Shock tube ignition delay experiments for NH_3 are quite sensitive to the rate constant for $NH_2 + O_2$. In Fig. 11, model predictions with the calculated rate constant and the chemical kinetic model discussed below are compared to data from Fujii et al. [86]. Sensitivity analysis for these conditions confirms that calculations of the NH_3 concentration as a function of time are primarily sensitive to the rate constant for $NH_2 + O_2$. The good agreement obtained supports the accuracy of the rate constant.

3. Chemical kinetic model

In this investigation, we use a detailed kinetic model to quantify the chemistry of the Thermal DeNO$_x$ process and the NNH mechanism for NO formation. The model is based on the reaction mechanism of Miller and Glarborg [22] for NH_3 oxidation and the Thermal DeNO$_x$ process. A number of changes to the mechanism were made, based on the present work (discussed above) as well as recent work of the authors [92–96]. Table 2 lists selected reactions; the full mechanism is available in the supplementary material.

The most important changes to the mechanism of Miller and Glarborg [22], based on the work outlined in the previous section, relate to the following reactions:

$$NNH = N_2 + H \quad (R33)$$

$$NNH + O = \text{products} \quad (R35\text{—}37)$$

$$NH_2 + O_2 = \text{products} \quad (R12, 13)$$

With the shorter lifetime for NNH of 10^{-9} s, the value of k_{33} has been increased by more than an order of magnitude. The overall rate constant for NNH + O is in the same range as used previously in modeling, but the channel to NH + NO is now considered to be minor, with k_{37} being substantially smaller than most previous estimates. Miller and Glarborg derived the $NH_2 + O_2$ rate constant based on an assumption of a very fast rate for the reverse step, $H_2NO + O$ (R12b). The present value of k_{12} is about an order of magnitude smaller, being more in line with the value from Dean and Bozzelli [67] used recently in modeling studies of NH_3 oxidation [92,94]. The novel rate coefficients for NH + NO = products (R26,27) and $N_2O + H = N_2 + OH$ (R60) are more in line with values used previously in modeling, even though they imply an increasing significance of the $NH + NO = N_2O + H$ reaction (R26) in forming and consuming N_2O.

In addition to the reactions of NNH discussed above, key steps include reactions of NH_2 and NH with NO and NO_2. The $NH_2 + NO$ reaction involves two product channels,

$$NH_2 + NO = N_2 + H_2O \quad (R14)$$

$$NH_2 + NO = NNH + OH \quad (R15)$$

Here the reaction numbers refer to the listing in Table 2. In particular the branching fraction for this reaction, defined as $\alpha = k_{15}/(k_{14} + k_{15})$, is important for model predictions of Thermal DeNO$_x$. In the present work, α was chosen to be consistent with the theoretical value of Miller and Klippenstein [16]. Their value for the branching fraction is slightly smaller than the recommendation of Miller and Glarborg [22] in the 1100–1400 K range, but it is in excellent agreement with a wide range of experimental determinations [5,11,12,14,15,18]. The overall rate constant for $NH_2 + NO$, $k_{NH_2+NO,tot}$, has been measured over a wide temperature range, and data agree roughly within a factor of 2. We retain $k_{NH_2+NO,tot}$ from previous modeling work [22]. A recent determination by Song et al. [97] indicates an overall rate constant that is about 25% smaller in the Thermal DeNO$_x$ temperature window than our present value, but this difference has only a minor impact on model predictions.

Similar to the $NH_2 + NO$ reaction, $NH_2 + NO_2$ has two product channels:

$$NH_2 + NO_2 = N_2O + H_2O \quad (R17)$$

$$NH_2 + NO_2 = H_2NO + NO \quad (R18)$$

For this reaction we select the overall rate constant from the work of Song et al. [98], together with a branching fraction $\beta = k_{17}/(k_{17} + k_{18})$ of 20% [20,98–100]. While the value of β is maintained from previous modeling work [22], it is worth noting that the overall rate constant of Song et al. is about a factor of 2 larger.

The NH + NO reaction system was discussed above. The $NH + NO_2$ reaction has only been characterized at low temperature. We have adopted the overall rate constant from the measurement of Harrison et al. [101] and the branching fraction between the two product channels, HNO + NO and $N_2O + OH$, from Quandt and Hershberger [102].

In addition to these changes, a few other rate constants were updated. Notably, rate coefficients for a number of reactions in the amine subset, including $NH_2 + OH$, were drawn from the recent theoretical work of Klippenstein et al. [96].

4. The Thermal DeNO$_x$ process

The Thermal DeNO$_x$ process was developed by Richard Lyon at EXXON in the early 1970s and published in 1975 [103]. It is a selective, non-catalytic reduction of NO (SNCR), using NH_3 as the reducing agent, and it is still widely used for NO_x control in combustion

of fuels such as biomass and waste, where catalytic cleaning may be prohibitive.

The chemistry of this process has been studied extensively, and a number of characteristic features have been identified [1,3,21,22,104]:

1. In the absence of combustibles, nitric oxide removal is possible only in a narrow temperature range centered at 1250 K. At temperatures below 1100 K, reaction is too slow to be significant, and above 1400 K the NH_3 is oxidized to NO rather than to N_2. In the temperature window for the process, the reaction is self-sustaining, i.e. it does not require addition of other fuel components to make it go.
2. The reaction requires oxygen to proceed below 1400 K. An increase in the oxygen concentration shifts the window towards lower temperatures and widens it.
3. Presence of combustibles such as H_2 or CO shifts the window for NO removal towards lower temperatures, and high combustible concentrations narrow the width of the window.
4. The reaction is not explosive. It takes place relatively smoothly in the course of about 0.1 s.

In a series of papers, Miller and co-workers explained these observations in terms of a sequence of elementary reactions [1,3,20–22]. Ammonia is converted to NH_2 by reaction with the O/H radical pool, primarily OH

$$NH_3 + OH = NH_2 + H_2O \quad (R4)$$

The following reaction between NH_2 and NO is the key step in the process. This reaction must simultaneously remove NO and produce free radicals to sustain reaction. It is well established that the reaction has two product channels [1],

$$NH_2 + NO = N_2 + H_2O \quad (R14)$$

$$NH_2 + NO = NNH + OH \quad (R15)$$

The subsequent reaction sequence, which is initiated by dissociation of NNH,

$$NNH = N_2 + H \quad (R33)$$

$$H + O_2 = O + OH$$

$$O + H_2O = OH + OH$$

secures that reaction (R15) leads to a net formation of three hydroxyl radicals. For the overall process to be self-sustainable, it is required that the branching fraction of the $NH_2 + NO$ reaction, defined as $\alpha = k_{15}/(k_{14} + k_{15})$ must be at least 25% [1]. While early experiments [4,6] indicated a smaller branching fraction, it is now well established that α in the 1100–1400 K range attains values of 0.3–0.4 [12,16,22].

The process is limited in the high temperature end by the chain branching cycle occurring too rapidly, thus leading to a strong growth in the O/H radical pool. This promotes conversion of NH_2 to NH,

$$NH_2 + OH = NH + H_2O, \quad (R9)$$

in competition with the $NH_2 + NO$ reaction (R14), (R15). Furthermore, the NH formed is partly oxidized to NO,

$$NH + O_2 = NO + OH \quad (R25)$$

$$NH + O_2 = HNO + O \quad (R24)$$

$$HNO + M = H + NO + M \quad (R41)$$

$$HNO + OH = NO + H_2O \quad (R44)$$

At sufficiently high temperatures, typically around 1400 K, this sequence leads to a net formation of NO.

The challenge in understanding the detailed chemistry of the Thermal $DeNO_x$ process concerns the lifetime and reactivity of NNH. When NNH is allowed to dissociate immediately, in line with the theoretical estimates of its lifetime, the reaction becomes explosive. Thus, the experimental observation that the system is non-explosive puts limitations on the NNH lifetime – a significant fraction of the NNH needs to react to form a less reactive species than atomic hydrogen. In the earlier models of Miller and coworkers [1,3], NNH was allowed to react with NO,

$$NNH + NO = N_2 + HNO \quad (R40)$$

At early reaction times, HNO dissociates thermally to form the H atom, but as the radical pool builds up, the chain terminating step

$$HNO + OH = NO + H_2O \quad (R44)$$

becomes competitive and limits the radical growth. The requirement from the modeling that NNH lives long enough to react with NO places a lower limit on the NNH lifetime of about 10^{-6} s [20], i.e. 2–3 orders of magnitude longer than the theoretical estimates discussed above.

The early experiments of Lyon and coworkers [105–107] indicated that NO_2 was not formed in the Thermal $DeNO_x$ process, pointing to a small rate constant for $NNH + O_2$ [1]. The detection of considerable amounts of NO_2 at higher oxygen concentrations [104] prompted Miller and Glarborg [21,22] to propose the reaction with O_2 as a major consumption step for NNH,

$$NNH + O_2 = N_2 + HO_2 \quad (R39)$$

The introduction of this reaction had several implications. First of all, it served to limit the chain branching, since HO_2 is much less reactive than H. Second, the subsequent reaction of HO_2 with NO,

$$NO + HO_2 = NO_2 + OH \quad (R54)$$

helped to explain the observation of NO_2 and established NO_2 as a key intermediate in the process. Part of the NO_2 is recycled to NO,

$$NH_2 + NO_2 = H_2NO + NO \quad (R18)$$

while part of it forms N_2O,

$$NH_2 + NO_2 = N_2O + H_2O \quad (R17)$$

Since O_2 is present in much larger quantities than NO in the process, the introduction of the $NNH + O_2$ reaction allowed the NNH lifetime to be shortened. While the best agreement between modeling and experiments was obtained with a lifetime of about 10^{-7} s [21], a value as low as 1.5×10^{-8} s was shown to be compatible with experiments [22].

In the present work, we use a value for the NNH lifetime of 10^{-9} s, fully consistent with the best theoretical predictions, as discussed above. A number of recent findings allow us to use such a small number and still maintain compatibility with experiment. Most importantly, the branching fraction α for the $NH_2 + NO$ reaction is smaller than those previously used in modeling. The branching fraction has now been measured quite accurately over a wide range of temperature using a variety of experimental techniques. The available data, supported by high-level theory, indicate a value of α that strongly limits chain branching in the temperature range 1100–1400 K. The high accuracy in the value of α, together with the improved rate coefficients for other key reactions, including $NH_2 + O_2$ and $NNH + O_2$ (this work), suggests that the remaining uncertainties in the Thermal $DeNO_x$ mechanism are quite small.

The major difference between the present mechanism and previous kinetic models for Thermal $DeNO_x$ is that the chain branching in the process is now mainly restricted by the small value of the branching fraction α of the $NH_2 + NO$ reaction, rather than by subsequent reactions of NNH with O_2 or NO. Actually, with the current

value of α proposed by Miller and Klippenstein [16], sufficient chain branching in the temperature window for the process can be maintained only if the lifetime of NNH is very short, of the order of 10^{-9} s.

To assess whether the current mechanism is consistent with the experimental findings for the Thermal DeNO$_x$ process, we evaluate the following key features of the process:

- The dependence on temperature.
- The dependence on oxygen concentration.
- The formation of NO_2 and N_2O.
- The impact of the presence of combustibles.
- The observation that the process is non-explosive.

Following Miller and Glarborg [21,22], the first three features, i.e. the temperature and [O_2] dependence and formation of NO_2 and N_2O, are illustrated by comparing model predictions to the experimental data of Kasuya et al. [104]. Kasuya et al. performed a series of Thermal DeNO$_x$ experiments in a flow reactor over a very wide range of O_2 concentrations, from 0.1% to 50%, and temperatures from 925 to 1375 K.

Figures 12–14 compare our model predictions for NO, NO_2, and N_2O, respectively, with the data of Kasuya et al. The comparisons shown are for a single set of initial concentrations for which Kasuya et al. obtained a complete set of data.

Figure 12 shows that the initiation temperature for the process decreases systematically as the inlet O_2 level increases. At the same time, the maximum amount of NO removal decreases, while the width of the temperature window increases. All these features are described satisfactorily by the model, even though the predicted temperature for onset of reaction is slightly shifted for some conditions. Specifically, the very short NNH lifetime of the present mechanism causes the predicted onset temperature to be less sensitive to the O_2 concentration in the range 4–50% than observed experimentally. A larger rate constant for the $NH_2 + O_2$ reaction, which may facilitate onset of reaction at high O_2 concentrations, would serve to enhance agreement with experiment. However, there is currently no support for a faster rate for this step.

Figure 13 shows how NO_2 is formed in significant quantities at the high concentrations of O_2, but the level drops off rapidly as O_2 decreases. These trends are described qualitatively by the model, even though the predicted window for NO_2 extends to higher temperatures than observed experimentally.

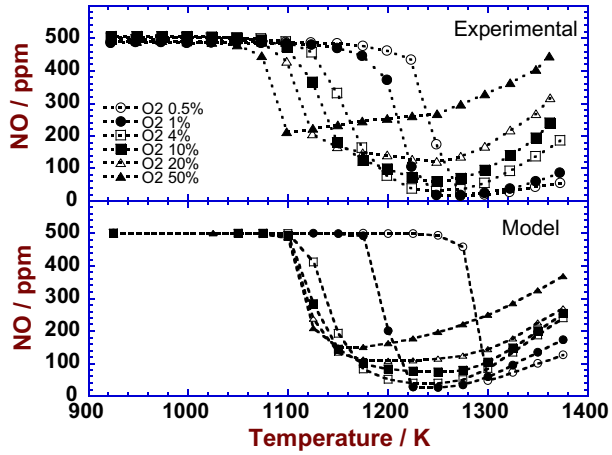

Fig. 12. Comparison of predictions of the present model with the experimental results of Kasuya et al. [104] for NO as a function of temperature and oxygen concentration in the Thermal DeNO$_x$ process. Inlet concentrations: NO = 500 ± 30 ppm, NH_3 = 1000 ± 60 ppm, H_2O = 5%, balance N_2. Residence time (s) = 88.0/T (T in Kelvin).

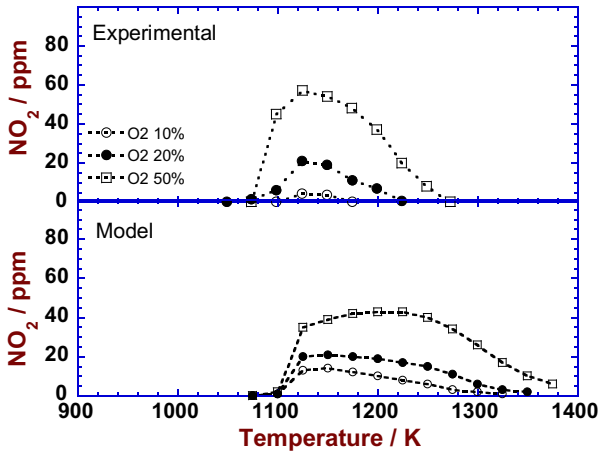

Fig. 13. Comparison of predictions of the present model with the experimental results of Kasuya et al. [104] for NO_2 as function of temperature and oxygen concentration in the Thermal DeNO$_x$ process. Inlet concentrations: NO = 500 ± 30 ppm, NH_3 = 1000 ± 60 ppm, H_2O = 5%, balance N_2. Residence time (s) = 88.0/T (T in Kelvin).

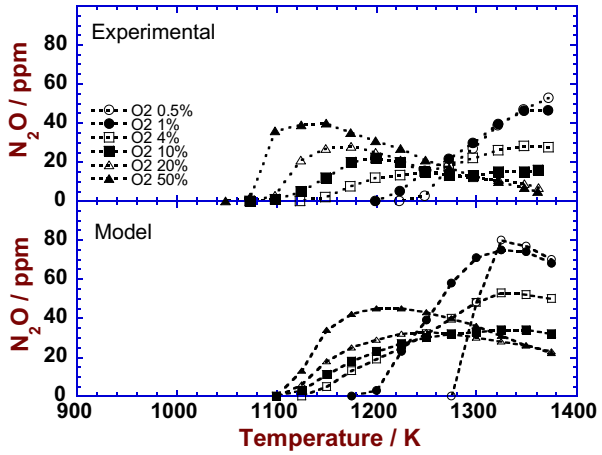

Fig. 14. Comparison of predictions of the present model with the experimental results of Kasuya et al. [104] for N_2O as a function of temperature and oxygen concentration in the Thermal DeNO$_x$ process. Inlet concentrations: NO = 500 ± 30 ppm, NH_3 = 1000 ± 60 ppm, H_2O = 5%, balance N_2. Residence time (s) = 88.0/T (T in Kelvin).

Due to the shorter lifetime of NNH in the present mechanism, $NNH + O_2$ is no longer the single dominant source of HO_2. Formation of HO_2, and thereby NO_2, is replenished through the sequence,

$$NH_2 + NO_2 = H_2NO + NO \quad (R18)$$

$$H_2NO + O_2 = HNO + HO_2 \quad (R52)$$

$$HNO + O_2 = NO + HO_2 \quad (R45)$$

$$NO + HO_2 = NO_2 + OH \quad (R54)$$

The competition between reactions of HNO and H_2NO with O_2 (neither of which are well characterized) and with the radical pool is important for the peak concentration of NO_2, as well as the width of the NO_2 formation window.

Figure 14 shows that the formation of N_2O is a complex function of temperature and oxygen concentration. The N_2O peak shifts from low temperature to high temperature as [O_2] increases. At 10% O_2, a double peak in N_2O can be detected, indicating that two mechanisms of N_2O formation are active. This is consistent

with the model predictions, as discussed by Miller and Glarborg [21,22]. The two sources of N_2O are the reactions

$$NH_2 + NO_2 = N_2O + H_2O \quad (R17)$$

active predominantly at lower temperatures and larger $[O_2]$ where NO_2 is readily available, and

$$NH + NO = N_2O + H \quad (R26)$$

which competes with $NH + O_2$ at higher temperatures and lower values of $[O_2]$. The predictions with the current mechanism agree qualitatively with the measured profiles, but the model overpredicts N_2O under conditions where the NH + NO reaction is the main source.

Figure 15 compares model predictions for the effect of H_2 addition on Thermal DeNO$_x$ with the experimental results of Duo et al. [108]. In line with a number of other experimental studies [107,109,110], the data of Duo et al. document that the presence of combustibles shifts the window for the process to lower temperatures by replenishing the radical pool. In addition to the shift in onset temperature, increasing amounts of combustibles also cause a narrowing of the process window. Both these effects are captured quite well by the model.

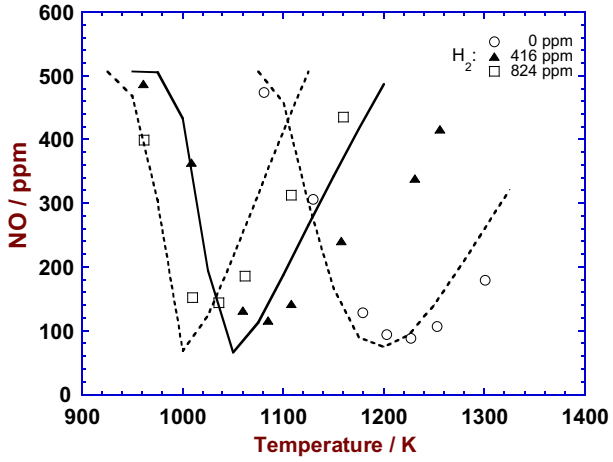

Fig. 15. Comparison of predictions of the present model with the experimental results of Duo et al. [108] for NO as a function of temperature and hydrogen concentration in the Thermal DeNO$_x$ process. Inlet mole fractions: NH_3 = 832 ppm, NO = 507 ppm, H_2 = 0/416/824 ppm, O_2 = 4.0%, H_2O = trace, balance N_2. Residence time (s) = 92.7/T (K).

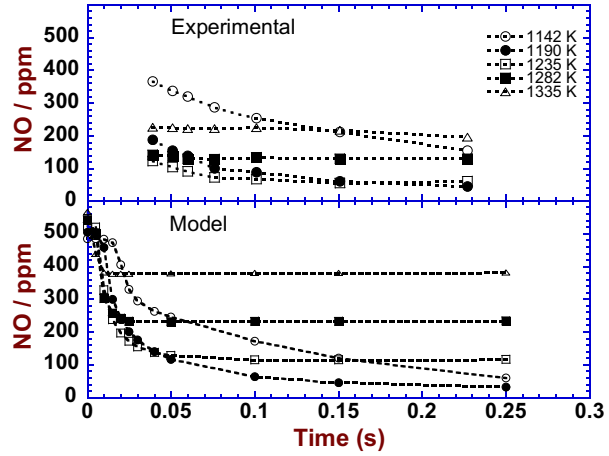

Fig. 16. Comparison of predictions of the present model with the experimental results of Duo et al. [111] for NO as a function of reaction time and temperature in the Thermal DeNO$_x$ process. Inlet concentrations (mol cm^{-3}): $[NH_3] = 8.45 \times 10^{-9}$, $[NO] = 5.15 \times 10^{-9}$, $[O_2] = 4.05 \times 10^{-5}$, $[H_2O]$ = trace, balance N_2. Note that the inlet mole fractions vary with temperature.

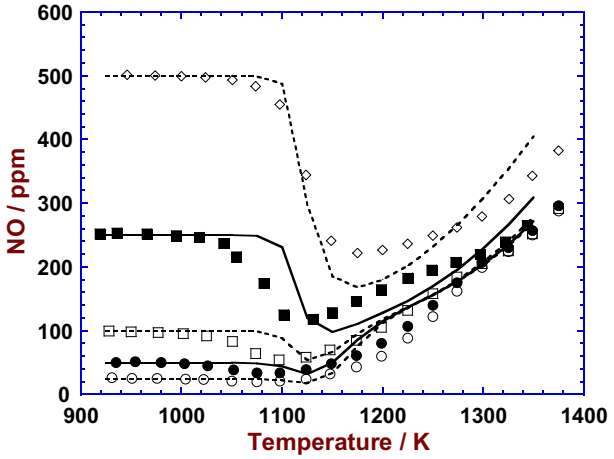

Fig. 17. Comparison of predictions of the present model with the experimental results of Vilas and Glarborg [112] for NO as a function of temperature and inlet NO concentration in oxidation of NH_3. Inlet mole fractions: NH_3 = 1000 ± 100 ppm, O_2 = 40 ± 1.2%, NO varying (25, 50, 100, 250, 500 ppm), H_2O = trace, balance N_2. Residence time (s) = 48.7/T (K).

Figure 16 shows NO profiles as a function of time and temperature for the Thermal DeNO$_x$ process. The measurements by Duo et al. [111] illustrate that at lower temperatures, below 1200 K, reaction progresses over a period of about 0.2 s, while at the highest temperature of 1335 K, reaction is completed within less than 40 ms. Even though there are some quantitative differences between the experimental results and the current model predictions, the transition from a slow to a fast regime is captured quite well by the model.

Figure 17 shows results for the transition from NH_3 oxidation to Thermal DeNO$_x$. In these experiments [112], the NH_3 and O_2 inlet levels were maintained at 1000 ppm and 40%, respectively, while the initial NO mole fraction was increased gradually from 25 ppm to 500 ppm. Several interesting features of this system

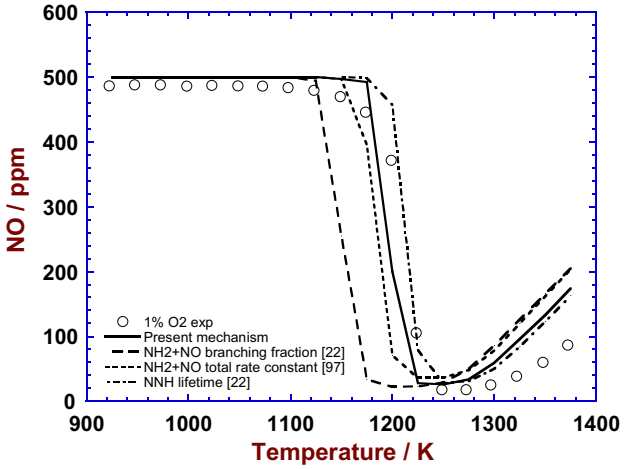

Fig. 18. Comparison of model predictions with the experimental results of Kasuya et al. [104] for NO as a function of temperature in the Thermal DeNO$_x$ process: impact of model parameters. Solid curve: present mechanism; long-dashed curve: branching fraction for NH_2 + NO from Miller and Glarborg [22]; short-dashed curve: total rate constant for NH_2 + NO from Song et al. [97]; dot-dashed line: NNH lifetime from Miller and Glarborg [22]. Inlet concentrations: NO = 500 ± 30 ppm, NH_3 = 1000 ± 60 ppm, O_2 = 1%, H_2O = 5%, balance N_2. Residence time (s) = 88.0/T (T in Kelvin).

are evident. Under conditions where the inlet NH_3 concentration is significantly greater than that of NO, i.e. for inlet levels of NO up to 250 ppm, the onset temperature for reaction is independent of the NO level. Even at the smallest NO concentration of 25 ppm, a minimum in NO is observed just above the initiation temperature, and inspection of the data shows that the fractional conversion of NO at the minimum is quite similar over the range of NO levels from 25 to 250 ppm. At higher temperatures (>1200 K), the exit NO concentration asymptotically approaches a common value, independent of the inlet level between 25 and 250 ppm. The model predictions capture all these trends well.

Figure 18 explores the sensitivity of the model predictions for Thermal $DeNO_x$ to the lifetime of NNH and the rate coefficient parameters for the NH_2 + NO reaction. Calculations are conducted for the conditions of the 1% O_2 experiment of Kasuya et al. [104]. The results show that under these conditions with a comparatively small [O_2], the most important model parameter is the branching fraction α for the NH_2 + NO reaction. The use of a slightly larger value of α, as preferred by Miller and Glarborg [22], results in a shift of the temperature window of more than 50 K. On the other hand, a decrease in the total rate constant for NH_2 + NO of about 25%, following Song et al. [97], or an increase in the NNH lifetime to 1.5×10^{-8}, following Miller and Glarborg [22], only have a minor impact on predictions under these conditions. Similar calculations for high [O_2] conditions, where the NNH + O_2 reaction is more competitive, reveal a much higher sensitivity to the NNH lifetime. It must be emphasized that the model predictions are so sensitive to the branching fraction for the NH_2 + NO reaction that even small changes, within the experimental uncertainty, have a large impact on the agreement of the model with the Thermal $DeNO_x$ experiments. However, once the branching fraction is fixed, only a narrow range of values for the NNH lifetime allows agreement between model predictions and experiment at high oxygen levels.

5. The NNH mechanism of NO formation

Several separate mechanisms have been identified that can lead to formation of nitrogen oxides from fixation of the molecular nitrogen contained in the combustion air. In the thermal (or Zel'dovich) NO mechanism, N_2 reacts with oxygen atoms [1] in the reaction O + N_2 = NO + N, followed by oxidation of the atomic nitrogen by O_2 or OH. The thermal mechanism requires temperatures above 1800 K and excess oxygen to be efficient. Prompt NO (or Fenimore NO) formation is initiated by attack of CH_i-radicals on N_2 forming cyanide species, which may subsequently be oxidized to NO [1]. Additional reaction paths to NO from atmospheric nitrogen are initiated by recombination of N_2 with atomic oxygen, O + N_2 (+M) = N_2O(+M) [113], or atomic hydrogen, H + N_2(+M) = NNH(+M) [24], followed by oxidation of the nitrogen intermediate to NO.

The NNH mechanism for forming NO consists of the reaction sequence [24],

$$N_2 + H = NNH \qquad (R33b)$$

$$NNH + O = NH + NO \qquad (R37)$$

$$NH + O_x = NO + \cdots$$

To attain significance in forming NO in combustion processes, this reaction sequence must secure a sufficient flux through the NNH + O reaction (R37). The key parameters in the mechanism are the lifetime of NNH, the heat of formation of NNH, and the rate constant k_{37} for NNH + O.

The lifetime of NNH is inversely proportional to the rate constant for the association reaction forming NNH (R33b). This step must be sufficiently fast to maintain a steady-state NNH level. With a lifetime of NNH of about 10^{-9} s, as used in the present model, both the formation and consumption of NNH are very fast, and thereby an NNH steady-state is rapidly attained. Since we are above the threshold at which the NNH formation rate is fast enough to maintain equilibrium, model predictions for NO formation through NNH are insensitive to the value of k_{33b}.

With the large rate constant for k_{33}, the yield of NO becomes proportional to the product $K_{P,33b} \times k_{37}$, in agreement with the analysis by Hayhurst and Hutchinson [28]. The steady-state concentration of NNH is determined by the equilibrium constant $K_{P,33b}$ for (R33b), which again depends on the heat of formation of NNH, $\Delta_f H_{298}$(NNH). If $\Delta_f H_{298}$(NNH) is in the high end of the reported range, the steady-state level of NNH and thereby the NO yield of the mechanism will be correspondingly lower. A change of 1.5 kcal mol^{-1} in the heat of formation of NNH corresponds roughly to a factor of 2 difference in the formation rate of NO [27]. The value of 59.6 kcal mol^{-1} from GRI-Mech [114], which has been used in most previous modeling studies, is consistent with the present value of $\Delta_f H_{298}$(NNH) = 59.7 kcal mol^{-1}. The value of 60.6 ± 0.5 kcal mol^{-1} from Haworth et al. [32] is slightly larger than the best current estimate, as discussed above.

Finally, the yield of NO from the NNH mechanism is directly proportional to the rate constant k_{37} for NNH + O = NH + NO. In most previous modeling studies this reaction has been assumed to be fast. Values are generally within a factor of 2 of the estimate from GRI-Mech [114] of 7×10^{13} cm^3 mol^{-1} s^{-1}. Bozzelli and Dean [24] estimated from QRRK theory a value of k_{37} of $3.3 \times 10^{14} T^{-0.23}$ exp(510/T) cm^3 mol^{-1} s^{-1}, while Konnov and coworkers [30,31] derived values of $(0.5–2) \times 10^{14}$ exp(−2000/T) cm^3 mol^{-1} s^{-1} from reinterpretation of data from jet-stirred reactors and flames. Our present rate constant for (R37) of $5.2 \times 10^{11} T^{0.388}$ exp(813/T) cm^3 mol^{-1} s^{-1}, as well as the recent theoretical value of $7.8 \times 10^{10} T^{0.642}$ exp(695/T) cm^3 mol^{-1} s^{-1} from Haworth et al. [32], are both considerably smaller, of the order of 1×10^{13} cm^3 mol^{-1} s^{-1} at 2000 K.

In order to quantify the formation of NO from the NNH mechanism, it is desirable to identify experimental conditions where the NNH scheme is the dominant source of NO. The N_2O scheme may be important at high pressure and moderate temperatures, while the NNH mechanism is most significant at lower temperatures or at short residence times and reducing conditions at higher temperatures [33,34]. There are indications that the NNH mechanism is most important in diffusion flames where NNH may form on the fuel-rich side of the flame sheet and then react with O inside the flame sheet [38]. However, we consider non-premixed flames less suited for kinetic interpretation due to the complications of the flow field. To exclude the possibility of prompt-NO formation, we limit our scope to non-hydrocarbon systems, i.e. with H_2 or H_2/CO mixtures as fuel. Reported experiments with these fuels, earlier used to quantify the NNH mechanism, include fuel-rich, low-pressure [27] and atmospheric pressure [28,31] flames, as well as lean stirred-reactor experiments [115,116].

In the present work, we have selected the low-pressure, fuel-rich flames of Harrington et al. [27] and the lean jet-stirred-reactor experiments of Steele et al. [115] for comparison with model predictions. The low-pressure H_2/air flames of Harrington et al. were designed to minimize formation of NO through thermal NO and N_2O mechanisms while yielding measurable quantities of NO from NNH. To obtain this condition, the flames were operated at comparatively low temperature (about 1200 K) and under reducing conditions.

In Fig. 19, the measured NO profiles from the two flames of Harrington et al., operated at 38 and 78 torr, respectively, are compared with model predictions. Calculations with the present mechanism (solid lines) are seen to substantially underpredict the NO level in both flames. The difference is more than an order

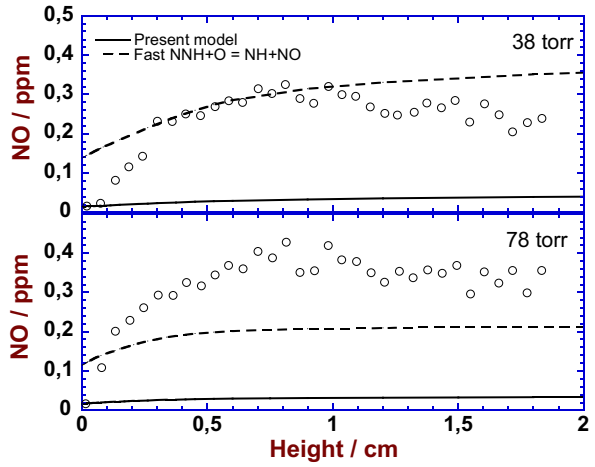

Fig. 19. Comparison of experimental LIF NO profiles of Harrington et al. [27] with predictions of the present model for two low-pressure H_2/air flames. Fuel/air equivalence ratio = 1.5, flame temperatures of the order of 1200 K.

of magnitude. The fact that the calculated NO levels are significantly below even those predicted by Haworth et al. [32] with a comparable value of k_{37} indicates that side reactions also play a role in the NO formation.

The dashed lines show model predictions with a high rate constant for NNH + O = NH + NO (R37). Here, we assume that (R37) proceeds with the calculated capture rate constant for the NNH + O reaction, i.e. that $k_{37} = k_{tot,NNH+O} \sim 8 \times 10^{13}$ cm^3 mol^{-1} s^{-1} and that $k_{35} = k_{36} = 0$. With the large value of k_{37}, the NO predictions are in much better agreement with experiment. However, it must be emphasized that this is an unreasonable rate constant for this reaction since the potential clearly indicates that NH + NO is a minor channel.

We currently cannot explain the difference between the observed and calculated NO levels for the flames of Harrington et al. However, it should be noted that they are heavily stabilized on the burner. Because of this, reactions occurring on the burner surface (or even inside the burner), such as recombination of hydrogen atoms, may have an impact on the species profiles in the early part of the flame. We find that model predictions are sensitive to assumptions about radical loss on the burner surface.

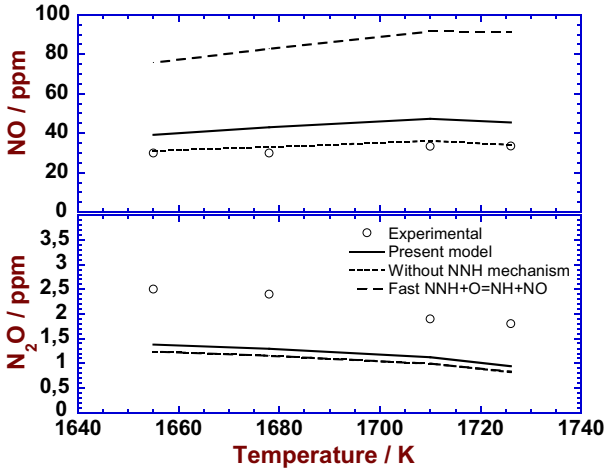

Fig. 20. Comparison of measured NO and N_2O profiles from combustion of CO/H_2 mixtures in the jet-stirred reactor of Steele et al. [115] with predictions of the present model. Results are shown as function of temperature with the following inlet composition: air/CO = 82/17.4 mol%, H_2 = 0.69–0.25 mol%. The residence time is in the range 3.87–4.03 ms. Short-dashed lines denote model predictions where the NNH mechanism has been deactivated by making the NNH dissociation irreversible, while long-dashed lines represent calculations with a fast rate constant for NNH + O = NH + NO ($k_{37} = k_{tot,NNH+O}$).

Malte and co-workers [113,115] have conducted a range of jet-stirred-reactor experiments to characterize NO formation in lean premixed combustion. While NO is mostly formed via N_2O under these conditions, Haworth et al. [32] identified the CO/H_2 oxidation data of Steele et al. [115] as being sensitive to NO formation from the NNH mechanism. Following Haworth et al., we have selected data from the experiments of Steele et al. for comparison with the model.

Figure 20 compares measured and predicted NO and N_2O concentrations as a function of temperature. The NO level is slightly overestimated by the model, while N_2O is underpredicted roughly by a factor of 2. If the NNH mechanism is deactivated by setting $k_{33b} = 0$, the predicted NO is reduced by about 25%, indicating that the NNH mechanism is less important than the N_2O mechanism under the conditions of these experiments. Modeling predictions with a fast rate constant for the NNH + O = NH + NO reaction ($k_{37} = k_{tot,NNH+O}$ and $k_{35} = k_{36} = 0$) leads to a substantial overprediction of NO, in agreement with the findings of Haworth et al. [32].

Since the low-pressure flames of Harrington et al. [27] may have been flawed by reactions on the burner surface due to heavy stabilization and the conditions of the lean jet-stirred-reactor experiments of Steele et al. [115] favor NO formation through N_2O rather than NNH, it is desirable with novel experimental results to quantify the NO formation through the NNH mechanism and to serve to validate the chemical kinetic model. However, we believe that the present mechanism provides a more accurate prediction of NO from NNH than previous models used in literature.

6. Conclusions

Model predictions for the Thermal DeNO$_x$ process and the NNH mechanism for NO formation rely heavily on the thermochemistry and reactions of NNH. In the present work, the heat of formation and the lifetime of NNH were evaluated based on a review of the literature. Furthermore, the NNH + O, NNH + O_2, and NH_2 + O_2 reaction systems were analysed using *ab initio* transition state theory based master-equation calculations incorporating high levels of electronic-structure theory and statistical rate theory. Based on this work, the NNH lifetime has been shortened to 10^{-9} s in the model, fully consistent with the best theoretical predictions, but more than an order of magnitude smaller than values used previously in modeling. While the overall reaction for NNH + O, as expected, was found to be very fast, the potential clearly indicates that NH + NO is a minor channel only, substantially smaller than most previous estimates.

The chemical kinetic model of Miller and Glarborg was updated with the findings discussed above, as well as with improved rate constants for a number of other steps including NNH + O_2 and NH_2 + O_2. With the present mechanism, the chain branching in the Thermal DeNO$_x$ process is now mainly restricted by the small value of the branching fraction α of the NH_2 + NO reaction, rather than by subsequent reactions of NNH with O_2 or NO. Experimental evidence, supported by high-level theory, indicates a value of α that strongly limits chain branching in the temperature range 1100–1400 K. The high accuracy in the value of α, together with the improved rate coefficients for the other key reactions suggests that the remaining uncertainties in the Thermal DeNO$_x$ mechanism are limited.

With NH + NO being only a minor channel for the NNH + O reaction, calculations with the present model for formation of NO via the NNH mechanism yield values that are substantially smaller than most earlier modeling studies, but our results are at least

qualitatively consistent with the work of Haworth et al. [32]. Available experimental results do not allow a quantification of the NNH mechanism, but we believe that the present mechanism allows a more accurate characterization than previous work.

Acknowledgments

The work at Argonne and Sandia was supported by the US Department of Energy, Office of Basic Energy Sciences, Division of Chemical Sciences, Geosciences, and Biosciences. The work at Argonne was supported under Contract No. DE-AC02-06CH11357. Sandia is a multiprogram laboratory operated by Sandia Corporation, a Lockheed Martin Company, for the United States Department of Energy's National Nuclear Security Administration under contract DE-AC04-94A18500. The work at DTU was funded by Energinet.dk as part of the Eranet Bioenergy program.

Appendix A. Supplementary material

Supplementary data associated with this article can be found, in the online version, at doi:10.1016/j.combustflame.2010.12.013.

References

[1] J.A. Miller, C.T. Bowman, Prog. Energy Combust. Sci. 15 (1989) 287–338.
[2] P. Glarborg, A.D. Jensen, J.E. Johnsson, Prog. Energy Combust. Sci. 29 (2003) 89–113.
[3] J.A. Miller, M.C. Branch, R.J. Kee, Combust. Flame 43 (1981) 81–98.
[4] B. Atakan, A. Jacobs, M. Wahl, R. Weller, J. Wolfrum, Chem. Phys. Lett. 155 (1989) 609–613.
[5] V.P. Bulatov, A.A. Ioffe, V.A. Lozovsky, O.M. Sarkisov, Chem. Phys. Lett. 161 (1989) 141–146.
[6] J.W. Stephens, C.L. Morter, S.K. Farhat, G.P. Glass, R.F. Curl, J. Phys. Chem. 97 (1993) 8944–8951.
[7] S.P. Walch, J. Chem. Phys. 99 (1993) 5295–5300.
[8] E.W. Diau, T. Yu, M.A.G. Wagner, M.C. Lin, J. Phys. Chem. 98 (1994) 4034–4042.
[9] J.A. Miller, Proc. Combust. Inst. 26 (1996) 461–480.
[10] E.W.G. Diau, S.C. Smith, J. Phys. Chem. 100 (1996) 12349–12354.
[11] J. Park, M.C. Lin, J. Phys. Chem. 100 (1996) 3317–3319.
[12] P. Glarborg, P.G. Kristensen, K. Dam-Johansen, J.A. Miller, J. Phys. Chem. A 101 (1997) 3741–3745.
[13] E.W.G. Diau, S.C. Smith, J. Chem. Phys. 106 (1997) 9236–9251.
[14] J. Park, M.C. Lin, J. Phys. Chem. 101 (1997) 5–13.
[15] J. Park, M.C. Lin, J. Phys. Chem. 103 (1999) 8906–8907.
[16] J.A. Miller, S.J. Klippenstein, J. Phys. Chem. A 104 (2000) 2061–2069.
[17] D.C. Fang, L.B. Harding, S.J. Klippenstein, J.A. Miller, Faraday Discuss. 119 (2001) 207–222.
[18] S.H. Song, R.K. Hanson, C.T. Bowman, D.M. Golden, J. Phys. Chem. A 106 (2002) 9233–9235.
[19] J.A. Miller, M.J. Pilling, J. Troe, Proc. Combust. Inst. 30 (2005) 43–88.
[20] P. Glarborg, K. Dam-Johansen, J.A. Miller, Int. J. Chem. Kinet. 27 (1995) 1207–1220.
[21] J.A. Miller, P. Glarborg, Springer Ser. Chem. Phys. 61 (1996) 318–333.
[22] J.A. Miller, P. Glarborg, Int. J. Chem. Kinet. 31 (1999) 757–765.
[23] C.C. Schmidt, C.T. Bowman, Combust. Flame 127 (2001) 1958–1970.
[24] J.W. Bozzelli, A.M. Dean, Int. J. Chem. Kinet. 27 (1995) 1097–1109.
[25] S.F. Selgren, P.W. McLoughlin, G.I. Gellene, J. Chem. Phys. 90 (1989) 1624–1629.
[26] U. Bozkaya, J.M. Turney, Y. Yamaguchi, H.F. Schaefer III, J. Chem. Phys. 132 (2010) 064308.
[27] J.E. Harrington, G.P. Smith, P.A. Berg, A.B. Noble, J.B. Jeffries, D.R. Crosley, Proc. Combust. Inst. 26 (1996) 2133–2138.
[28] A.N. Hayhurst, E.M. Hutchinson, Combust. Flame 114 (1998) 274–279.
[29] A.A. Konnov, G. Colson, J. De Ruyck, Combust. Flame 121 (2000) 548–550.
[30] A.A. Konnov, J. De Ruyck, Combust. Flame 125 (2000) 1258–1264.
[31] A.A. Konnov, I.V. Dyakov, J. De Ruyck, Proc. Combust. Inst. 20 (2002) 2171–2177.
[32] N.L. Haworth, J.C. Mackie, G.B. Bacskay, J. Phys. Chem. A 107 (2003) 6792–6803.
[33] A.A. Konnov, Combust. Flame 134 (2003) 421–424.
[34] A. Frassoldati, T. Faravelli, E. Ranzi, Int. J. Hydrogen Energy 31 (2006) 2310–2328.
[35] M. Skottene, K.E. Rian, Int. J. Hydrogen Energy 32 (2007) 3572–3585.
[36] J.B. Bell, M.S. Day, X. Gao, P. Glarborg, Numerical Simulation of nitrogen oxide formation in lean premixed turbulent $H_2/O_2/N_2$ flames, Proc. Combust. Inst. 33 (2011) 1591–1599.
[37] D.D. Thomsen, N.M. Laurendeau, Combust. Flame 124 (2001) 350–369.
[38] J.B. Bell, M.S. Day, J.F. Grcar, W.G. Bessler, C. Schulz, P. Glarborg, A. Jensen, Proc. Combust. Inst. 29 (2002) 2195–2202.
[39] N. Sullivan, A. Jensen, P. Glarborg, M.S. Day, J.F. Grcar, J.B. Bell, C.J. Pope, R.J. Kee, Combust. Flame 131 (2002) 285–298.
[40] H.S. Guo, G.J. Smallwood, F.S. Liu FS, Y.G. Ju, O.L. Gulder, Proc. Combust. Inst. 30 (2005) 303–311.
[41] T. Rutar, J.C.Y. Lee, P. Dagaut, P.C. Malte, A.A. Byrne, Proc. Inst. Mech. Eng. A–J. Power Energy 221 (2007) 387–398.
[42] C. Galletti, A. Parente, M. Derudi, R. Rota, L. Tognotti, J. Hydrogen Energy 34 (2009) 8339–8351.
[43] J.A. Miller, S.J. Klippenstein, J. Phys. Chem. A 110 (2006) 10528–10544.
[44] J.A. Miller, S.J. Klippenstein, J. Phys. Chem. A 107 (2003) 2680–2692.
[45] S.J. Klippenstein, J.A. Miller, J. Phys. Chem. A 106 (2002) 9267–9277.
[46] J.A. Miller, S.J. Klippenstein, S.H. Robertson, J. Phys. Chem. A 104 (2000) 7525–7536;
J.A. Miller, S.J. Klippenstein, S.H. Robertson, J. Phys. Chem. A 104 (2000) 9806.
[47] A. Fernandez-Ramos, J.A. Miller, S.J. Klippenstein, D.G. Truhlar, Chem. Rev. 106 (2006) 4518–4584.
[48] J.A. Miller, S.J. Klippenstein, S.H. Robertson, M.J. Pilling, N.J.B. Green, Phys. Chem. Chem. Phys 11 (2009) 1128–1137.
[49] S.J. Klippenstein, Y. Georgievskii, L.B. Harding, Phys. Chem. Chem. Phys. 8 (2006) 1133–1147.
[50] S.J. Klippenstein, L.B. Harding, A.W. Jasper, Phys. Chem. Chem. Phys. 9 (2007) 4055–4070.
[51] L.B. Harding, Y. Georgievskii, S.J. Klippenstein, J. Phys. Chem. A 109 (2005) 4646–4656.
[52] MOLPRO, Version 2009.1, a package of ab initio programs, H.-J. Werner, P.J. Knowles, R. Lindh, F.R. Manby, M. Schütz, P. Celani, T. Korona, A. Mitrushenkov, G. Rauhut, T.B. Adler, R.D. Amos, A. Bernhardsson, A. Berning, D.L. Cooper, M.J.O. Deegan, A.J. Dobbyn, F. Eckert, E. Goll, C. Hampel, G. Hetzer, G. Knizia, C. Köppl, Y. Liu, A.W. Lloyd, R.A. Mata, A.J. May, S.J. McNicholas, W. Meyer, M.E. Mura, A. Nicklaß, P. Palmieri, K. Pflüger, R. Pitzer, M. Reiher, U. Schumann, H. Stoll, A.J. Stone, R. Tarroni, T. Thorsteinsson, M. Wang, A. Wolf, <www.molpro.net>.
[53] L.A. Curtiss, D.L. Drapcho, J.A. Pople, Chem. Phys. Lett. 103 (1984) 437–442.
[54] S.P. Walch, R.J. Duchovic, C.M. Rohlfing, J. Chem. Phys. 90 (1989) 3230–3240.
[55] S.P. Walch, J. Chem. Phys. 93 (1990) 2384–2392.
[56] H. Koizumi, G.C. Schatz, S.P. Walch, J. Chem. Phys. 95 (1991) 4130–4135.
[57] S.P. Walch, J. Chem. Phys. 95 (1991) 4277–4283.
[58] S.P. Walch, H. Partridge, Chem. Phys. Lett. 233 (1995) 331–334.
[59] G. Li, H. Guo, Chem. Phys. Lett. 347 (2001) 443–450.
[60] Y. Guo, D.L. Thompson, J. Chem. Phys. 116 (2002) 3670–3675.
[61] Y. Guo, D.L. Thompson, J. Chem. Phys. 118 (2003) 3096–3101.
[62] L.A. Poveda, A.J.C. Varandas, J. Phys. Chem. A 107 (2003) 7923–7930.
[63] P.J.S.B. Caridade, S.P.J. Rodrigues, F. Sousa, A.J.C. Varandas, J. Phys. Chem. A 109 (2005) 2356–2363.
[64] T. Stoecklin, A. Voronin, Chem. Phys. 331 (2007) 385–395.
[65] P.J.S.B. Caridade, L.A. Poveda, S.P.J. Rodrigues, A.J.C. Varandas, J. Phys. Chem. A 111 (2007) 1172–1178.
[66] V.C. Mota, A.J.C. Varandas, J. Phys. Chem. A 112 (2008) 3768–3786.
[67] A.M. Dean, J.W. Bozzelli, in: W.C. Gardiner (Ed.), Gas-Phase Combustion Chemistry, Springer, New York, 2000, pp. 125–343.
[68] H.-J. Werner, Mol. Phys. 89 (1996) 645–661.
[69] P. Celani, H.-J. Werner, J. Chem. Phys. 112 (2000) 5546–5557.
[70] R.A. Kendall, T.H. Dunning Jr., R.J. Harrison, J. Chem. Phys. 96 (1992) 6796–6806.
[71] S.J. Klippenstein, J. Chem. Phys. 96 (1992) 367–371.
[72] Y. Georgievskii, S.J. Klippenstein, J. Phys. Chem. A 107 (2003) 9776–9781.
[73] D.L. Baulch, C.T. Bowman, C.J. Cobos, R.A. Cox, T. Just, J.A. Kerr, M.J. Pilling, D. Stocker, J. Troe, W. Tsang, R.W. Walker, J. Warnatz, J. Phys. Chem. Ref. Data 34 (2005) 757–1397.
[74] P. Marshall, A. Fontijn, C.F. Melius, J. Chem. Phys. 86 (1987) 5540–5549.
[75] A.W. Jasper, J.A. Miller, J. Phys. Chem. A 113 (2009) 5612–5619.
[76] A.W. Jasper, J.A. Miller, Predictive unimolecular kinetics for $CH_4 + M \rightleftarrows CH_3 + H + M$ in eight baths: M = He, Ne, Ar, Kr, H_2, CO, N_2, and CH_4. J. Phys. Chem. A, in preparation.
[77] J.A. Miller, S.J. Klippenstein, Phys. Chem. Chem. Phys. 6 (2004) 1192–1202.
[78] J.P. Senosiain, S.J. Klippenstein, J.A. Miller, J. Phys. Chem. A 110 (2006) 5772–5781.
[79] J.P. Senosiain, S.J. Klippenstein, J.A. Miller, J. Phys. Chem. A 110 (2006) 6960–6970.
[80] S.R. Sellevåg, Y. Georgievskii, J.A. Miller, J. Phys. Chem. A 112 (2008) 5085–5095.
[81] S.J. Klippenstein, J.A. Miller, J. Phys. Chem. A 109 (2005) 4285–4295.
[82] J.P. Senosiain, S.J. Klippenstein, J.A. Miller, J. Phys. Chem. A 109 (2005) 6045–6055.
[83] J.A. Miller, S.J. Klippenstein, C. Raffy, J. Phys. Chem. A 106 (2002) 4904–4913.
[84] S.R. Sellevåg, Y. Georgievskii, J.A. Miller, J. Phys. Chem. A 113 (2009) 4457–4467.
[85] J.A. Miller, J.P. Senosiain, S.J. Klippenstein, Y. Georgievskii, J. Phys. Chem. A 112 (2008) 9429–9438.
[86] N. Fujii, H. Miyama, M. Koshi, T. Asaba, Proc. Combust. Inst. 18 (1981) 873–883.
[87] J.V. Michael, R.B. Klemm, W.D. Brobst, S.R. Bosco, D.F. Nava, J. Phys. Chem. 89 (1985) 3335.

[88] G.S. Tyndall, J.J. Orlando, K.E. Nickerson, C.A. Cantrell, J.G. Calvert, J. Geophys. Res. 96 (1991) 20761.
[89] V.A. Lozovsky, O.M. Sarkisov, A.G. Okhrimchuk, A.L. Enis, Chem. Phys. Rep. 16 (1997) 395–417.
[90] C. F. Melius, J. S. Binkley, in T. M. Sloane, Ed. The Chemistry of Combustion Processes, ACS Symp. Series 249 (1984) 103-115.
[91] R. Sumathi, S.D. Peyerimhoff, J. Chem. Phys. 108 (1998) 5510–5521.
[92] Ø. Skreiberg, P. Kilpinen, P. Glarborg, Combust. Flame 136 (2004) 501–518.
[93] C.L. Rasmussen, J. Hansen, P. Marshall, P. Glarborg, Int. J. Chem. Kinet. 40 (2008) 454–480.
[94] Z. Tian, Y. Li, L. Zhang, P. Glarborg, F. Qi, Combust. Flame 156 (2009) 1413–1426.
[95] T. Mendiara, P. Glarborg, Combust. Flame 156 (2009) 1937–1949.
[96] S.J. Klippenstein, L.B. Harding, B. Ruscic, R. Sivaramakrishnan, N.K. Srinivasan, M.-C. Su, J.V. Michael, J. Phys. Chem. A 113 (2009) 10241–10259.
[97] S.H. Song, R.K. Hanson, C.T. Bowman, D.M. Golden, Int. J. Chem. Kinet. 33 (2001) 715–721.
[98] S.H. Song, D.M. Golden, R.K. Hanson, C.T. Bowman, Proc. Combust. Inst. 29 (2002) 2163–2170.
[99] R.W. Quandt, J.F. Hershberger, J. Phys. Chem. 100 (1996) 9407–9411.
[100] J. Park, M.C. Lin, J. Phys. Chem. A 101 (1997) 2643–2647.
[101] J.A. Harrison, A.R. Whyte, L.F. Phillips, Chem. Phys. Lett. 129 (1986) 346–352.
[102] R.W. Quandt, J.F. Hershberger, J. Phys. Chem. 99 (1995) 16939–16944.
[103] R.K. Lyon, US Patent 3900,554, 1975.
[104] F. Kasuya, P. Glarborg, K. Dam-Johansen, Chem. Eng. Sci. 50 (1995) 1455–1466.
[105] R.K. Lyon, Int. J. Chem. Kinet. 8 (1976) 315–318.
[106] R.K. Lyon, D. Benn, Proc. Combust. Inst. 17 (1979) 601.
[107] R.K. Lyon, J.E. Hardy, Ind. Eng. Chem. Fundam. 25 (1986) 19–24.
[108] W. Duo, K. Dam-Johansen, K. Østergaard, The Influence of Additives on Selective Non-Catalytic Reduction of Nitroc Oxide with Ammonia, Paper Presented ACHEMASIA '89, Beijing, China, October 11–17, 1989.
[109] S.L. Chen, J.C. Kramlich, W.R. Seeker, D.W. Pershing, J. Air Waste Manage. Assoc. 39 (1989) 1375–1379.
[110] M.U. Alzueta, H. Røjel, P.G. Kristensen, P. Glarborg, K. Dam-Johansen, Energy Fuels 11 (1997) 716–723.
[111] W. Duo, K. Dam-Johansen, K. Østergaard, Can. J. Chem. Eng. 70 (1992) 1014–1020.
[112] E. Vilas, P. Glarborg, The selective non-catalytic reduction of NO with ammonia at high oxygen concentration, CHEC Report R0410, DTU Chemical Engineering, Technical University of Denmark, 2800 Kgs. Lyngby, Denmark, 2004.
[113] P.C. Malte, D.T. Pratt, Proc. Combust. Inst. 15 (1975) 1061–1070.
[114] G.P. Smith, D.M. Golden, M. Frenklach, N.W. Moriarty, B. Eiteneer, M. Goldenberg, C.T. Bowman, R.K. Hanson, S. Song, W.C. Gardiner, V.V. Lissianski, Z. Qin, GRI-MECH v3.0, <http://www.me.berkeley.edu/gri_mech/>.
[115] R.C. Steele, P.C. Malte, D.G. Nicol, J.C. Kramlich, Combust. Flame 100 (1995) 440–449.
[116] L. Xie, S. Hayashi, K. Hirose, Proc. Combust. Inst. 26 (1996) 2155.